JHEP

Published for SISSA by Springer

Received: August 25, 2016
Accepted: September 9, 2016
Published: September 23, 2016

Neutrino mass, dark matter and anomalous magnetic moment of muon in a $\mathrm{U}(1)_{L_\mu - L_\tau}$ model

Anirban Biswas,[a] **Sandhya Choubey**[a,b] **and Sarif Khan**[a]

[a] *Harish-Chandra Research Institute,*
Chhatnag Road, Jhunsi, Allahabad 211 019, India
[b] *Department of Theoretical Physics, School of Engineering Sciences,*
KTH Royal Institute of Technology,
AlbaNova University Center, 106 91 Stockholm, Sweden

E-mail: anirbanbiswas@hri.res.in, sandhya@hri.res.in, sarifkhan@hri.res.in

Abstract: The observation of neutrino masses, mixing and the existence of dark matter are amongst the most important signatures of physics beyond the Standard Model (SM). In this paper, we propose to extend the SM by a local $L_\mu - L_\tau$ gauge symmetry, two additional complex scalars and three right-handed neutrinos. The $L_\mu - L_\tau$ gauge symmetry is broken spontaneously when one of the scalars acquires a vacuum expectation value. The $L_\mu - L_\tau$ gauge symmetry is known to be anomaly free and can explain the beyond SM measurement of the anomalous muon $(g-2)$ through additional contribution arising from the extra $Z_{\mu\tau}$ mediated diagram. Small neutrino masses are explained naturally through the Type-I seesaw mechanism, while the mixing angles are predicted to be in their observed ranges due to the broken $L_\mu - L_\tau$ symmetry. The second complex scalar is shown to be stable and becomes the dark matter candidate in our model. We show that while the $Z_{\mu\tau}$ portal is ineffective for the parameters needed to explain the anomalous muon $(g-2)$ data, the correct dark matter relic abundance can easily be obtained from annihilation through the Higgs portal. Annihilation of the scalar dark matter in our model can also explain the Galactic Centre gamma ray excess observed by Fermi-LAT. We show the predictions of our model for future direct detection experiments and neutrino oscillation experiments.

Keywords: Neutrino Physics, Beyond Standard Model, Cosmology of Theories beyond the SM

ArXiv ePrint: 1608.04194

doi:10.1007/JHEP09(2016)147

JHEP09(2016)147

Contents

1 Introduction 1

2 Model 4

3 Muon ($g-2$) 7

4 Neutrino masses and mixing 9

5 Dark matter 14

5.1 Relic density 14

5.2 Direct detection 15

5.3 Results 17

5.4 Indirect detection: Fermi-LAT γ-ray excess from the galactic centre 20

6 Summary and conclusion 21

1 Introduction

Explaining of the origin of nonzero neutrino masses and dark matter (DM) are two of the principal challenges which theoretical high energy physics has been facing over the last few decades. Neutrinos were predicted to be massless in the Standard Model (SM) of particle physics. However, in 1998 the neutrino oscillation (oscillation between mass and flavour eigenstates) which requires nonzero mass differences between different generation of neutrinos and mixing between them, was unambiguously observed by the Super-Kamiokande atmospheric neutrino experiment [2]. Existence of neutrino mass and mixing requires the extension of the SM. Neutrino oscillations have now been established at a very high confidence level by many outstanding experimental observations by experiments such as SNO [3] (solar neutrino experiment), KamLand [4] (reactor neutrino experiment), Daya Bay [5], RENO [6], Double Chooz [7] (reactor neutrino experiments with short baselines), NOνA [10, 11] (accelerator neutrino experiments). At present for normal (inverted) mass ordering scenarios, the best fit values [12] of neutrino oscillation parameters obtained from global neutrino oscillation data are:[1]

$$\Delta m^2_{21} = 7.37 \times 10^{-5}\ \text{eV}^2, \quad |\Delta m^2_{\text{atm}}| = 2.50\,(2.46) \times 10^{-5}\ \text{eV}^2$$
$$\theta_{12} = 33.02^\circ, \qquad \theta_{23} = 41.38^\circ\,(48.97^\circ), \qquad \theta_{13} = 8.41^\circ\,(8.49^\circ) \quad (1.1)$$

[1]We define $\Delta m^2_{ij} = m^2_i - m^2_j$. The mass squared difference $\Delta m^2_{\text{atm}} = m^2_3 - ((m^2_2 + m^2_1)/2)$, where we use the notation given in [12].

JHEP09(2016)147

On other hand, the existence of dark matter in the Universe has been confirmed to a very high statistical significance by many indirect evidences such as the flatness of rotation curves of spiral galaxies [13], collision of galaxies in a galaxy cluster (bullet cluster and others) [14, 15], gravitational lensing [16] and the measurements of the Cosmic Microwave Background (CMB) [17, 18]. The satellite borne CMB experiments, WMAP [17] and Planck [18], have measured the fractional contribution of dark matter to the present energy density of the Universe (commonly known as DM relic density) to be around 0.25 with an extremely good accuracy, while the contribution of the visible baryonic matter is only around 0.05. The rest $\sim 70\%$ of energy density of the Universe is also coming from an mysterious energy called the Dark Energy [19]. The current best observed value of DM relic density is [18]

$$\Omega_{\rm DM}h^2 = 0.1197 \pm 0.0022\,. \tag{1.2}$$

Like the neutrino sector mentioned before, the SM of particle physics does not have any stable particle(s) which can play the role of viable DM candidate(s). Therefore beyond Standard Model (BSM) scenario is required to explain these two long standing puzzles. Weakly Interacting Massive Particles (WIMP) [20, 21] have been proposed as one of the most promising candidates to explain the dark matter puzzle of the Universe. Many direct detection experiments like LUX [22], XENON [23] and CDMS [24] have been trying to detect WIMPs through their spin independent as well as spin dependent elastic scattering with the detector nuclei. However, no convincing signature of WIMPs has been observed yet in the direct detection experiments, giving bounds on the WIMP-nucleon scattering cross section. Recently, the LUX collaboration has reported the most stringent upper bound on DM-nucleon spin independent scattering cross section to be around 2.2×10^{-46} $\rm cm^{-2}$ [25] for a $\sim 50\,\rm GeV$ DM particle.

Signature of DM can also appear in indirect detection experiments, looking for high energy neutrinos, gamma rays and charged cosmic rays (electrons, positrons, protons and antiprotons) coming from the annihilation or decay of DM particles [26]. In this work, we will briefly discuss about the Galactic Centre gamma-ray excess in the energy range 1-3 GeV which has been observed by the Fermi-LAT collaboration [27]. Although, there are some astrophysical explanations such as unresolved point sources (e.g. millisecond pulsar) [28, 29] for this excess gamma-ray flux, but in this work we will explain this anomalous excess by the process of DM annihilation into $b\bar{b}$ final state. The authors of ref. [30] have given constraints on DM mass and its annihilation cross section $\langle\sigma \rm v_{b\bar{b}}\rangle$ to explain the gamma-ray excess which are $48.7^{+6.4}_{-5.2}\,\rm GeV$ and $1.75^{+0.28}_{-0.26}\times 10^{-26}\ \rm cm^3/s$ for the $b\bar{b}$ annihilation channel respectively. In the present model we can explain this excess gamma-ray flux in the energy range 1-3 GeV.

The SM has accidental U(1) global symmetries like the baryon (B) and the lepton number (L) conservation. However, if we want to convert these global symmetries into a local one then they become anomalous. The anomaly free situation can be obtained if instead of considering B and L separately one uses some combinations between them. There are only four non-anomalous combinations possible, and these are $B-L$, L_e-L_μ, $L_\mu-L_\tau$ and L_e-L_τ where L_e, L_μ and L_τ are the respective lepton numbers of generations associated with leptons e, μ and τ while $L = L_e + L_\mu + L_\tau$ is the total lepton number. Out

JHEP09(2016)147

of these four possible combinations, axial vector anomaly [31, 32] and gravitational gauge anomaly [33, 34] of local $B-L$ symmetric models can be cancelled by the introduction of extra chiral fermions to the SM such as three right handed neutrinos [35] or two left and right handed singlet fermions with appropriate $B-L$ charges [36]. However, unlike the $B-L$ case, the anomaly cancellation does not require any extra chiral fermionic degrees of freedom for the last three cases where the linear combinations of different generational lepton numbers [37–39] are considered. Here anomalies cancel between different leptonic generations. Among these three possible scenarios $\mathrm{U}(1)_{L_\mu - L_\tau}$ extension [40–69] of SM is less constrained as in this case the extra neutral gauge boson does not couple to electron and quarks and therefore $Z_{\mu\tau}$ is free from any constraints coming from lepton and hadron colliders such as LEP [70, 71] and LHC [72]. Therefore, the mass of $Z_{\mu\tau}$ can be as light as $\mathcal{O}$ (100 MeV) for a low value of gauge coupling $g_{\mu\tau} \lesssim 10^{-3}$ which is required to satisfy the constraints arising from neutrino trident production [73]. One of the phenomenological motivation for the $\mathrm{U}(1)_{L_\mu - L_\tau}$ extension of the SM is that it can explain the muon $(g-2)$ anomaly between the theoretical value predicted by the SM [74] which is $a_\mu^{\mathrm{th}} = 1.1659179090(65) \times 10^{-3}$ and the experimental value [75] which is $a_\mu^{\mathrm{exp}} = 1.16592080(63) \times 10^{-3}$. The difference between theoretical and experimantal value [75] is,

$$\Delta a_\mu = a_\mu^{\mathrm{exp}} - a_\mu^{\mathrm{th}} = (29.0 \pm 9.0) \times 10^{-10}\,. \tag{1.3}$$

In this work, we have considered the gauged $\mathrm{U}(1)_{L_\mu - L_\tau}$ extension of the SM. Amongst the main motivations for our choice of this model is that it provides $\mu - \tau$ flavor symmetry which could naturally explain the peculiar neutrino mixing parameters (cf. eq. (1.1)) wherein θ_{23} is close to maximal and θ_{13} is small. As mentioned above, this model can also explain the muon $(g-2)$ anomaly [77–81] for a range of $Z_{\mu\tau}$ mass and $g_{\mu\tau}$ consistent with collider constraints. We will further extend this model with a complex scalar, which will become a viable DM candidate. $\mathrm{U}(1)_{L_\mu - L_\tau}$ extended Ma model [82] has been studied earlier in the context of small neutrino mass generation in one loop level [83] and dark matter [84]. A review on earlier works about $\mu - \tau$ flavour symmetry in neutrino sector can be found in [40] and references therein. In order to generate neutrino masses through the Type-I seesaw mechanism [85–88] in the present scenario, we have introduced three right handed neutrinos (N_e, N_μ, N_τ) with $L_\mu - L_\tau$ charges 0, 1 and -1 respectively in the fermionic sector of SM. The scalar sector of the model is also enlarged by the addition of two complex scalar singlets (ϕ_H and ϕ_{DM}) with nonzero $L_\mu - L_\tau$ charge. The proposed $L_\mu - L_\tau$ symmetry is broken spontaneously when ϕ_H acquires vacuum expectation value (VEV) $v_{\mu\tau}$ and thereby making $Z_{\mu\tau}$ massive. The breaking of $L_\mu - L_\tau$ symmetry also results in additional terms in the neutrino mass matrix. In particular, the $\mu - \tau$ symmetry is broken and we can generate neutrino masses and mixing parameters consistent with current bounds. We show that the complex scalar ϕ_{DM} is stable in our model and hence becomes the DM candidate satisfying the constraints from Planck, LUX and LHC results. We show that a sub-region of the parameter space that is consistent with Planck, LUX and LHC results can also explain the Galactic Centre gamma ray excess observed by Fermi-LAT.

The rest of the article is organised as follows. In section 2, we describe the model for the present work. In section 3 and section 4 we discuss muon $(g-2)$ and neutrino masses

JHEP09(2016)147

Gauge	Baryon Fields			Lepton Fields			Scalar Fields		
Group	$Q_L^i = (u_L^i, d_L^i)^T$	u_R^i	d_R^i	$L_L^i = (\nu_L^i, e_L^i)^T$	e_R^i	N_R^i	ϕ_h	ϕ_H	$\phi_{\rm DM}$
$\rm SU(2)_L$	2	1	1	2	1	1	2	1	1
$\rm U(1)_Y$	1/6	2/3	−1/3	−1/2	−1	0	1/2	0	0

Table 1. Particle contents and their corresponding charges under SM gauge group.

and mixing angles, respectively. In section 5 we study the DM constraints and its related phenomenology. In section 6 we conclude.

2 Model

In this present work, we have considered a minimal extension of the SM where we have imposed an extra local $\rm U(1)_{L_\mu - L_\tau}$ symmetry to the SM Lagrangian, where L_μ and L_τ denote the muon lepton number and tau lepton number respectively. Therefore, the Lagrangian of the present model remains invariant under the $\rm SU(3)_c \times SU(2)_L \times U(1)_Y \times U(1)_{L_\mu - L_\tau}$ gauge symmetry. This model is free from axial vector and mixed gravitational gauge anomalies as these anomalies cancel between second and third generations of leptons without the requirement of any additional chiral fermion. The full particle content of our model and their respective charges under $\rm SU(2)_L \times U(1)_Y \times U(1)_{L_\mu - L_\tau}$ gauge groups are listed in tables 1 and 2. In order to break the $\rm U(1)_{L_\mu - L_\tau}$ symmetry spontaneously, we need a complex scalar field ϕ_H with a non-trivial $L_\mu - L_\tau$ charge assignment such that the $L_\mu - L_\tau$ symmetry is broken spontaneously when ϕ_H picks up a vacuum expectation value $v_{\mu\tau}$. Spontaneous breaking of the $L_\mu - L_\tau$ symmetry generates mass for the extra neutral gauge boson $Z_{\mu\tau}$. It has been shown that the spontaneously broken $L_\mu - L_\tau$ model can explain the anomalous muon $g-2$ signal. The $L_\mu - L_\tau$ symmetry is a flavor symmetry and hence can be used to explain the peculiar mixing pattern of the neutrinos [89]. In our model we generate small neutrino masses through the Type-I seesaw mechanism. To that end we introduce three right handed neutrinos (N_e, N_μ, N_τ) with $L_\mu - L_\tau$ charges of 0, 1 and −1 respectively, such that their presence do not introduce any further anomaly. In the $\rm U(1)_{L_\mu - L_\tau}$ symmetric limit the right-handed neutrino mass has exact $\mu - \tau$ symmetry. We will show that the spontaneous breaking of the gauged $\rm U(1)_{L_\mu - L_\tau}$ symmetry leads to additional terms in the right-handed neutrino mass matrix, providing a natural explanation of the neutrino masses and mixing parameters observed in neutrino oscillation experiments, given in eq. (1.1). We also add another complex scalar field $\phi_{\rm DM}$ in the model, with a chosen $L_\mu - L_\tau$ charge $n_{\mu\tau}$ such that the Lagrangian does not contain any term with odd power of $\phi_{\rm DM}$. Also the scalar field $\phi_{\rm DM}$ does not acquire any VEV and consequently in this model $\phi_{\rm DM}$ becomes odd under a remnant $\mathbb{Z}_2$ symmetry after the spontaneous breaking of the gauged $\rm U(1)_{L_\mu - L_\tau}$ symmetry, which ensure its stability. Hence $\phi_{\rm DM}$ can be a viable dark matter candidate.

We now write the Lagrangian of present model, which is given by

$$\mathcal{L} = \mathcal{L}_{\rm SM} + \mathcal{L}_N + \mathcal{L}_{\rm DM} + (D_\mu \phi_H)^\dagger (D^\mu \phi_H) - V(\phi_h, \phi_H) - \frac{1}{4} F^{\alpha\beta}_{\mu\tau} F_{\mu\tau_{\alpha\beta}}\,, \tag{2.1}$$

Gauge Group	Baryonic Fields	Lepton Fields			Scalar Fields		
	(Q_L^i, u_R^i, d_R^i)	(L_L^e, e_R, N_R^e)	$(L_L^\mu, \mu_R, N_R^\mu)$	$(L_L^\tau, \tau_R, N_R^\tau)$	ϕ_h	ϕ_H	$\phi_{\rm DM}$
$\mathrm{U}(1)_{L_\mu - L_\tau}$	0	0	1	-1	0	1	$n_{\mu\tau}$

Table 2. Particle contents and their corresponding charges under $\mathrm{U}(1)_{L_\mu - L_\tau}$.

where $\mathcal{L}_{\rm SM}$ is the usual SM Lagrangian while the Lagrangian for the right handed neutrinos containing their kinetic energy terms, mass terms and Yukawa terms with the SM lepton doublets, is denoted by $\mathcal{L}_N$ which can be written as

$$\begin{aligned}\mathcal{L}_N = & \sum_{i=e,\,\mu,\,\tau} \frac{i}{2}\bar{N}_i\gamma^\mu D_\mu N_i - \frac{1}{2}\,M_{ee}\,\bar{N}_e^c N_e - \frac{1}{2}\,M_{\mu\tau}\,(\bar{N}_\mu^c N_\tau + \bar{N}_\tau^c N_\mu) \\ & -\frac{1}{2}\,h_{e\mu}(\bar{N}_e^c N_\mu + \bar{N}_\mu^c N_e)\phi_H^\dagger - \frac{1}{2}\,h_{e\tau}(\bar{N}_e^c N_\tau + \bar{N}_\tau^c N_e)\phi_H \\ & - \sum_{i=e,\,\mu,\,\tau} y_i \bar{L}_i \tilde{\phi}_h N_i + h.c. \end{aligned} \tag{2.2}$$

with $\tilde{\phi}_h = i\,\sigma_2\phi_h^*$ and M_{ee}, $M_{\mu\tau}$ are constants having dimension of mass while the Yukawa couplings $h_{e\mu}$, $h_{e\tau}$ and y_i are dimensionless constants. In eq. (2.1), $\mathcal{L}_{\rm DM}$ represents the dark sector Lagrangian including the interactions of $\phi_{\rm DM}$ with other scalar fields. The expression of $\mathcal{L}_{\rm DM}$ is given by

$$\begin{aligned}\mathcal{L}_{\rm DM} = & (D^\mu\phi_{\rm DM})^\dagger(D_\mu\phi_{\rm DM}) - \mu_{\rm DM}^2\phi_{\rm DM}^\dagger\phi_{\rm DM} - \lambda_{\rm DM}(\phi_{\rm DM}^\dagger\phi_{\rm DM})^2 \\ & -\lambda_{Dh}(\phi_{\rm DM}^\dagger\phi_{\rm DM})(\phi_h^\dagger\phi_h) - \lambda_{DH}(\phi_{\rm DM}^\dagger\phi_{\rm DM})(\phi_H^\dagger\phi_H)\,. \end{aligned} \tag{2.3}$$

Moreover, the quantity $V(\phi_h, \phi_H)$ in eq. (2.1) contains all the self interaction of ϕ_H and its interaction with SM Higgs doublet. Therefore,

$$V(\phi_h, \phi_H) = \mu_H^2\phi_H^\dagger\phi_H + \lambda_H(\phi_H^\dagger\phi_H)^2 + \lambda_{hH}(\phi_h^\dagger\phi_h)(\phi_H^\dagger\phi_H)\,. \tag{2.4}$$

The expressions of all the covariant derivatives appearing in eqs. (2.1)–(2.3) can be written in a generic form which is given as

$$D_\nu X = (\partial_\nu + i\,g_{\mu\tau}\,Q_{\mu\tau}(X)\,Z_{\mu\tau_\nu})\,X\,, \tag{2.5}$$

where X is any field which is singlet under SM gauge group but has a $L_\mu - L_\tau$ charge $Q_{\mu\tau}(X)$ (see table 2) and $g_{\mu\tau}$ is the gauge coupling of the $\mathrm{U}(1)_{L_\mu - L_\tau}$ group. Furthermore, the last term in eq. (2.1) represents the kinetic term for the extra neutral gauge boson $Z_{\mu\tau}$ in terms of its field strength tensor $F_{\mu\tau}^{\alpha\beta} = \partial^\alpha Z_{\mu\tau}^\beta - \partial^\beta Z_{\mu\tau}^\alpha$.

The $L_\mu - L_\tau$ symmetry breaks spontaneously when ϕ_H acquires VEV and consequently the corresponding gauge field $Z_{\mu\tau}$ becomes massive, $M_{Z_{\mu\tau}} = g_{\mu\tau}\,v_{\mu\tau}$. In the unitary gauge, the expressions of ϕ_h and ϕ_H after spontaneous breaking of the $\mathrm{SU}(2)_{\rm L}\times\mathrm{U}(1)_{\rm Y}\times\mathrm{U}(1)_{L_\mu - L_\tau}$ gauge symmetry are

$$\phi_h = \begin{pmatrix} 0 \\ \dfrac{v+H}{\sqrt{2}} \end{pmatrix}\,, \qquad \phi_H = \left(\frac{v_{\mu\tau} + H_{\mu\tau}}{\sqrt{2}}\right)\,, \tag{2.6}$$

JHEP09(2016)147

where v and $v_{\mu\tau}$ are the VEVs of ϕ_h and ϕ_H respectively. Presence of the mutual interaction term in eq. (2.4) between ϕ_h and ϕ_H introduces mass mixing between the scalar fields H and $H_{\mu\tau}$. The scalar mass matrix with off-diagonal elements proportional to λ_{hH} is given by

$$\mathcal{M}^2_{\text{scalar}} = \begin{pmatrix} 2\lambda_h\, v^2 & \lambda_{hH}\, v_{\mu\tau}\, v \\ \lambda_{hH}\, v_{\mu\tau}\, v & 2\lambda_H\, v^2_{\mu\tau} \end{pmatrix} . \tag{2.7}$$

From the expression of $\mathcal{M}^2_{\text{scalar}}$ it is evident that if $\lambda_{hH} = 0$ (i.e. the interaction between ϕ_h and ϕ_H is absent), there is no mixing between H and $H_{\mu\tau}$ and hence they can represent two physical states. In our model however $\lambda_{hH} \neq 0$ and consequently the states representing the physical scalars will be obtained after the diagonalization of matrix $\mathcal{M}^2_{\text{scalar}}$. The new physical states which are linear combinations of H and $H_{\mu\tau}$ can be written as

$$\begin{aligned} h_1 &= H\cos\alpha + H_{\mu\tau}\sin\alpha\,, \\ h_2 &= -H\sin\alpha + H_{\mu\tau}\cos\alpha\,. \end{aligned} \tag{2.8}$$

The mixing angle α and the corresponding eigenvalues (masses of h_1 and h_2) are given by

$$\tan 2\alpha = \frac{\lambda_{hH}\, v_{\mu\tau}\, v}{\lambda_h v^2 - \lambda_H v^2_{\mu\tau}}\,, \tag{2.9}$$

$$M^2_{h_1} = \lambda_h v^2 + \lambda_H v^2_{\mu\tau} + \sqrt{(\lambda_h v^2 - \lambda_H v^2_{\mu\tau})^2 + (\lambda_{hH}\, v\, v_{\mu\tau})^2}\,, \tag{2.10}$$

$$M^2_{h_2} = \lambda_h v^2 + \lambda_H v^2_{\mu\tau} - \sqrt{(\lambda_h v^2 - \lambda_H v^2_{\mu\tau})^2 + (\lambda_{hH}\, v\, v_{\mu\tau})^2}\,. \tag{2.11}$$

We have considered h_1 as the SM-like Higgs boson[2] which has recently been discovered by ATLAS [90] and CMS [91] collaborations. Therefore its mass M_{h_1} and VEV v are kept fixed at 125.5 GeV and 246 GeV respectively. The mass of dark matter candidate ϕ_{DM} takes the following form

$$M^2_{\text{DM}} = \mu^2_{\text{DM}} + \frac{\lambda_{Dh}\, v^2}{2} + \frac{\lambda_{DH}\, v^2_{\mu\tau}}{2}\,. \tag{2.12}$$

In this model our ground state is defined as $\langle\phi_h\rangle = \dfrac{v}{\sqrt{2}}$, $\langle\phi_H\rangle = \dfrac{v_{\mu\tau}}{\sqrt{2}}$ and $\langle\phi_{\text{DM}}\rangle = 0$ this requires

$$\mu^2_h < 0,\ \ \mu^2_H < 0 \text{ and } \mu^2_{\text{DM}} > 0. \tag{2.13}$$

The stability of the ground state (vacuum) requires the following inequalities [92] among

[2] Eq. (2.10), (2.11) are valid when $M_{h_1} > M_{h_2}$. On the other hand, the expressions of M_{h_1} and M_{h_2} will be interchanged for $M_{h_2} > M_{h_1}$ resulting an change in sign to the mixing angle α.

JHEP09(2016)147

the quartic couplings of scalar fields

$$\begin{aligned}
&\lambda_h \geq 0, \lambda_H \geq 0, \lambda_{\rm DM} \geq 0,\\
&\lambda_{hH} \geq -2\sqrt{\lambda_h\,\lambda_H},\\
&\lambda_{Dh} \geq -2\sqrt{\lambda_h\,\lambda_{\rm DM}},\\
&\lambda_{DH} \geq -2\sqrt{\lambda_H\,\lambda_{\rm DM}},\\
&\sqrt{\lambda_{hH}+2\sqrt{\lambda_h\,\lambda_H}}\sqrt{\lambda_{Dh}+2\sqrt{\lambda_h\,\lambda_{\rm DM}}}\sqrt{\lambda_{DH}+2\sqrt{\lambda_H\,\lambda_{\rm DM}}}\\
&+2\,\sqrt{\lambda_h\lambda_H\lambda_{\rm DM}}+\lambda_{hH}\sqrt{\lambda_{\rm DM}}+\lambda_{Dh}\sqrt{\lambda_H}+\lambda_{DH}\sqrt{\lambda_h}\geq 0\quad .
\end{aligned}\tag{2.14}$$

Besides the above inequalities, the upper bound on quartic, gauge and Yukawa couplings can be obtained from the condition of perturbativity. For a scalar quartic coupling λ ($\lambda = \lambda_h,\ \lambda_H,\ \lambda_{\rm DM},\ \lambda_{hH},\ \lambda_{Dh},\ \lambda_{DH}$) this condition will be ensured when [93]

$$\lambda < 4\pi\,, \tag{2.15}$$

while for gauge coupling $g_{\mu\tau}$ and Yukawa coupling y ($y = y_e,\ y_\mu,\ y_\tau,\ h_{e\mu}$ and $h_{e\tau}$) it is [93]

$$g_{\mu\tau},\ y < \sqrt{4\pi}\,. \tag{2.16}$$

The above quadratic and quartic couplings of scalars fields ϕ_h and ϕ_H namely μ_h^2, μ_H^2, λ_h, λ_H and λ_{hH} can be expressed in terms of physical scalar masses (M_{h_1}, M_{h_2}), mixing angle α and VEVs (v, $v_{\mu\tau}$), which have been given in [92].

3 Muon ($g-2$)

It is well known that from the Dirac equation, the magnetic moment of muon $\vec{M}$ can be written in terms of its spin ($\vec{S}$), which is

$$\vec{M} = g_\mu \frac{e}{2\,m_\mu}\vec{S}, \tag{3.1}$$

where m_μ is the mass of muon and $g_\mu = 2$ is the gyromagnetic ratio. However, if we calculate g_μ using QFT then contributions arising from loop corrections slightly shift the value of g_μ from 2. Hence one can define a quantity a_μ which describes the deviation of g_μ from its tree level value,

$$a_\mu = \frac{g_\mu - 2}{2}\,. \tag{3.2}$$

In general, the contribution to the theoretical value of a_μ ($a_\mu^{\rm th}$) comes from the following sources [74]

$$a_\mu^{\rm th} = a_\mu^{\rm QED} + a_\mu^{\rm EW} + a_\mu^{\rm Had}\,, \tag{3.3}$$

where the contributions arising from Quantum Electrodynamics (QED), Electroweak theory and hadronic process are denoted by $\mathrm{a}_\mu^{\rm QED}$, $\mathrm{a}_\mu^{\rm EW}$ and $\mathrm{a}_\mu^{\rm Had}$ respectively. The SM prediction of a_μ including the above terms is [75]

$$a_\mu^{\rm th} = 1.1659179090(65)\times 10^{-3}\,. \tag{3.4}$$

JHEP09(2016)147

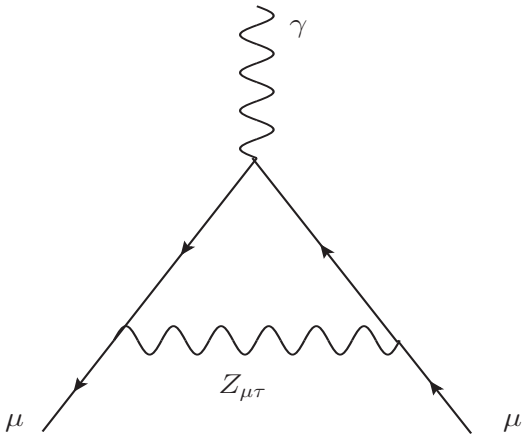

Figure 1. One loop Feynman diagram contributing to muon $(g-2)$, mediated by the extra gauge boson $Z_{\mu\tau}$.

On the other hand, a_μ has been precisely measured experimentally, initially by the CERN experiments and later on by the E821 experiment, and the current average experimental value is [78]

$$a_\mu^{\rm exp} = 1.16592080(63) \times 10^{-3}\,. \tag{3.5}$$

From the above one can see that although the theoretically predicted and the experimentally measured values of a_μ are quite close to each other, there still exists some discrepancy between these two quantities at the 3.2σ significance which is [75],

$$\Delta a_\mu = a_\mu^{\rm exp} - a_\mu^{\rm th} = (29.0 \pm 9.0) \times 10^{-10}\,. \tag{3.6}$$

Therefore, in order to reduce the difference between $a_\mu^{\rm exp}$ and $a_\mu^{\rm th}$ we need to explore BSM scenarios where we can get extra contributions from some extra diagrams. In our $\mathrm{U}(1)_{L_\mu - L_\tau}$ model we have an additional one loop diagram compared to the SM, which is mediated by the extra neutral gauge boson $Z_{\mu\tau}$ and gives nonzero contribution to $a_\mu^{\rm th}$ as shown in figure 1. The additional contribution to $a_\mu^{\rm th}$ from this diagram is given by [76, 77],

$$\Delta a_\mu(Z_{\mu\tau}) = \frac{g_{\mu\tau}^2}{8\pi^2} \int_0^1 dx \frac{2x(1-x)^2}{(1-x)^2 + rx}\,, \tag{3.7}$$

where, $r = (M_{Z_{\mu\tau}}/m_\mu)^2$ is the square of the ratio between masses of gauge boson $(Z_{\mu\tau})$ and muon. As mentioned in the Introduction, although a $\mathcal{O}(100\,\mathrm{MeV})$ $Z_{\mu\tau}$ is allowed, its coupling strength $(g_{\mu\tau})$ is strongly constrained to be less than $\sim 10^{-3}$ from the measurement of neutrino trident cross section by experiments like CHARM-II [94] and CCFR [95]. In our analysis, we find that for $M_{Z_{\mu\tau}} = 100\,\mathrm{MeV}$ and $g_{\mu\tau} = 9 \times 10^{-4}$ the value of $\Delta a_\mu = 22.6 \times 10^{-10}$, which lies around the ballpark value given in eq. (3.6). In what follows, we will use $M_{Z_{\mu\tau}} = 100\,\mathrm{MeV}$ and $g_{\mu\tau} = 9.0 \times 10^{-3}$ as our benchmark point for the analyses of neutrino masses and dark matter phenomenology.

JHEP09(2016)147

4 Neutrino masses and mixing

Majorana neutrino masses are generated via the Type-I seesaw mechanism by the addition of three right handed neutrinos to the model. Using eq. (2.2) we can write the Majorana mass matrix for the three right handed neutrinos as

$$\mathcal{M}_R = \begin{pmatrix} M_{ee} & \frac{v_{\mu\tau}}{\sqrt{2}} h_{e\mu} & \frac{v_{\mu\tau}}{\sqrt{2}} h_{e\tau} \\ \frac{v_{\mu\tau}}{\sqrt{2}} h_{e\mu} & 0 & M_{\mu\tau}\, e^{i\xi} \\ \frac{v_{\mu\tau}}{\sqrt{2}} h_{e\tau} & M_{\mu\tau}\, e^{i\xi} & 0 \end{pmatrix}, \tag{4.1}$$

where all parameters in M_R in general can be complex. However, by proper phase rotation one can choose all the elements expect the $\mu\tau$ component of M_R to be real [83]. Thus, M_R depends on the real parameters M_{ee}, $M_{\mu\tau}$, $h_{e\mu}$ and $h_{e\tau}$ and the phase ξ. On other hand, from the Yukawa term in eq. (2.2) one can easily see that the Dirac mass matrix M_D between left handed and right handed neutrinos is diagonal and for simplicity we have chosen all the Yukawa couplings (y_e, y_μ and y_τ) are real. The expression of M_D is

$$M_D = \begin{pmatrix} f_e & 0 & 0 \\ 0 & f_\mu & 0 \\ 0 & 0 & f_\tau \end{pmatrix}, \tag{4.2}$$

where $f_i = \dfrac{y_i}{\sqrt{2}} v$ with $i = e$, μ and τ. Now, with respect to the basis $\left(\overline{\nu_{\alpha L}} \;\; \overline{(N_{\alpha R})^c}\right)^T$ and $((\nu_{\alpha L})^c \;\; N_{\alpha R})^T$ we can write the mass matrix of both left as well as right handed neutrinos which is given as

$$M = \begin{pmatrix} 0 & M_D \\ M_D^T & M_R \end{pmatrix}, \tag{4.3}$$

where M is a 6×6 matrix and both M_D and M_R are 3×3 matrices given by eqs. (4.1) and (4.2). After diagonalisztion of the matrix M one obtains two fermionic states for each generation which are Majorana in nature. Therefore we have altogether six Majorana neutrinos, out of which three are light and rest are heavy. Using block diagonalisation technique, we can find the mass matrices for light as well as heavy neutrinos which are given as

$$m_\nu \simeq -M_D\, M_R^{-1} M_D^T, \tag{4.4}$$

$$m_N \simeq M_R\,. \tag{4.5}$$

Here both m_ν and m_N are complex symmetric matrices. Also eqs. (4.4)–(4.5) are derived using an assumption that $M_D \ll M_R$ i.e. the eigenvalues of M_D is much less than those of

JHEP09(2016)147

M_R and therefore terms with higher powers of M_D/M_R are neglected. Using the expressions of M_R and M_D given in eqs. (4.1)–(4.2) the light neutrino mass matrix in this model takes the following form

$$m_\nu = \frac{1}{2\,p}\begin{pmatrix} 2\,f_e^2 M_{\mu\tau}^2 e^{i\xi} & -\sqrt{2}\,f_e f_\mu\,h_{e\tau} v_{\mu\tau} & -\sqrt{2}\,f_e f_\tau\,h_{e\mu} v_{\mu\tau} \\ -\sqrt{2}\,f_e f_\mu\,h_{e\tau} v_{\mu\tau} & \dfrac{f_\mu^2\,h_{e\tau}^2\,v_{\mu\tau}^2\,e^{-i\xi}}{M_{\mu\tau}} & \dfrac{f_\mu\,f_\tau}{M_{\mu\tau}}(M_{ee}\,M_{\mu\tau} - p\,e^{-i\xi}) \\ -\sqrt{2}\,f_e f_\tau\,h_{e\mu} v_{\mu\tau} & \dfrac{f_\mu\,f_\tau}{M_{\mu\tau}}(M_{ee}\,M_{\mu\tau} - p\,e^{-i\xi}) & \dfrac{f_\tau^2\,h_{e\mu}^2\,v_{\mu\tau}^2\,e^{-i\xi}}{M_{\mu\tau}} \end{pmatrix}, \quad (4.6)$$

where $p = h_{e\mu}\,h_{e\tau}\,v_{\mu\tau}^2 - M_{ee}\,M_{\mu\tau}\,e^{i\xi}$. The masses and mixing angles of the light neutrinos are found by diagonalising this matrix [96] and are compared against the corresponding experimentally allowed ranges obtained from global analysis of the data (cf. eq. (1.1)).

There are eight independent parameters in the light neutrino mass matrix m_ν, namely, f_e, f_μ, f_τ, $M_{\mu\tau}$, M_{ee}, $V_{e\tau} = \frac{v_{\mu\tau}}{\sqrt{2}}\,h_{e\tau}$, $V_{e\mu} = \frac{v_{\mu\tau}}{\sqrt{2}}\,h_{e\mu}$ and ξ. All of these parameters have mass dimension GeV except the dimensionless phase factor ξ which is in radian. In order to find the model parameter space allowed by the neutrino oscillation experiments, we have varied the above mentioned parameters in the following range

$$\begin{aligned} 0 \leq \xi\,[\text{rad}] &\leq 2\pi\ , \\ 1 \leq M_{ee},\,M_{\mu\tau}\,[\text{GeV}] &\leq 10^4\ , \\ 1 \leq V_{e\mu},\ \ V_{e\tau}\ \ [\text{GeV}] &\leq 280\ , \\ 0.1 \leq \frac{(f_e,\,f_\mu,\,f_\tau)}{10^{-4}}\,[\text{GeV}] &\leq 10\ . \end{aligned} \quad (4.7)$$

The allowed parameter space satisfies the following constraints from the neutrino sector

- cosmological upper bound on the sum of all three light neutrinos, $\sum_i m_i < 0.23\,\text{eV}$ at 2σ C.L. [18],
- mass squared differences $6.93 < \dfrac{\Delta m_{21}^2}{10^{-5}}\,\text{eV}^2 < 7.97$ and $2.37 < \dfrac{\Delta m_{31}^2}{10^{-3}}\,\text{eV}^2 < 2.63$ in 3σ range [12],
- all three mixing angles $30^\circ < \theta_{12} < 36.51^\circ$, $37.99^\circ < \theta_{23} < 51.71^\circ$ and $7.82^\circ < \theta_{13} < 9.02^\circ$ also in 3σ range [12].

All the Yukawa couplings appearing in the light as well as heavy Majorana neutrino mass matrices (m_ν and M_R) are enforced to always lie within the perturbative range mentioned in eq. (2.16). Furthermore, we scan the allowed areas in the model parameter space for only for the normal mass ordering which corresponds to $\Delta m_{31}^2 > 0$.

In the left and right panels of figure 2, we have shown the allowed regions in $f_e - f_\mu$ and $f_e - f_\tau$ planes respectively, where we have varied f_e, f_μ, f_τ in the range $10^{-5}\,\text{GeV}$ to $10^{-3}\,\text{GeV}$ while the other parameters have been scanned over the entire considered range as given in eq. (4.7). From both the panels it is clear that there is (anti)correlation between the parameters $f_e - f_\mu$ and $f_e - f_\tau$. We find that for the lower values of f_e higher values

JHEP09(2016)147

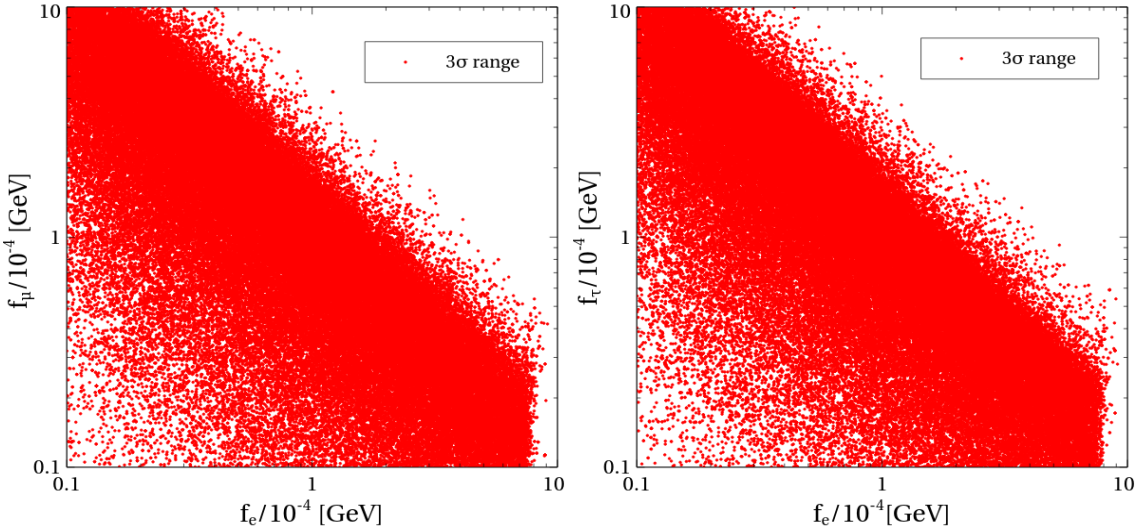

Figure 2. Left (Right) panel: allowed region in $f_e - f_\mu$ ($f_e - f_\tau$) plane which satisfies all the experimental constraints considered in this work.

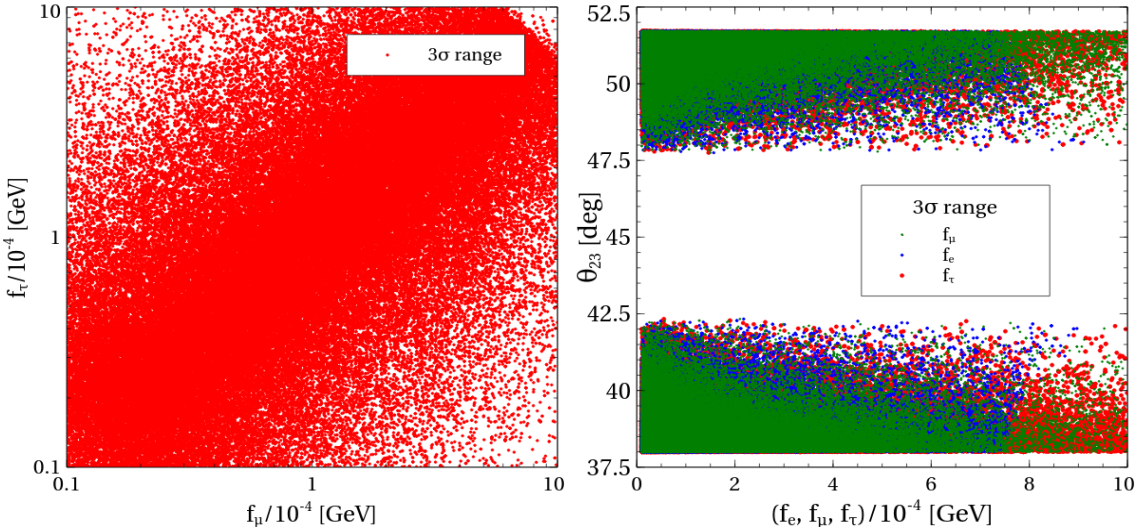

Figure 3. Left panel: allowed region in $f_\mu - f_\tau$ plane. Right panel: variation of θ_{23} with f_e (blue dots), f_μ (green dots) and f_τ (red dots).

of f_μ, f_τ are needed to satisfy the experimental constraints in the 3σ range and vice versa. Moreover, although there are smaller number of allowed points when both f_e and f_i ($i = \mu$, τ) are small but the present experimental bounds on the observables of the neutrino sector forbid the entire region in the $f_e - f_\mu$ and $f_e - f_\tau$ planes for both f_e and $f_i > 2 \times 10^{-4}$ GeV ($i = \mu$, τ). Also, unlike the parameters f_μ and f_τ, we do not get any allowed values of f_e beyond 8×10^{-4} GeV.

The allowed parameter space in $f_\mu - f_\tau$ plane has been shown in the left panel of figure 3. From the figure it is seen that there is a correlation between the parameters f_μ and f_τ. That means unlike the previous plots here most of allowed points in $f_\mu - f_\tau$ plane

JHEP09(2016)147

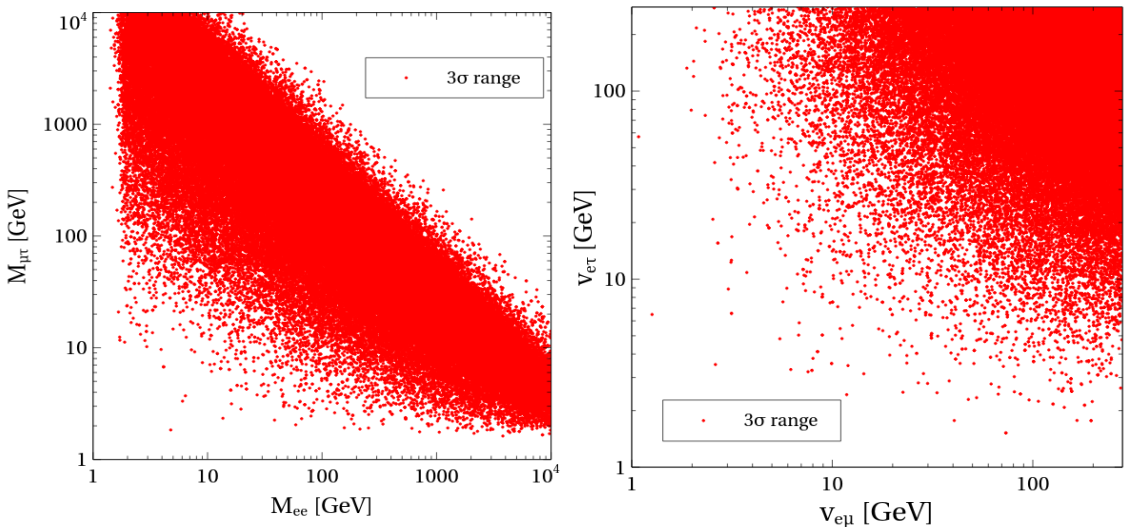

Figure 4. Left (Right) panel: allowed region in $M_{ee} - M_{\mu\tau}$ ($V_{e\mu} - V_{e\tau}$) plane which satisfies all the experimental constraints considered in this work.

are such that for the lower (higher) values of the parameter f_μ we also need lower (higher) values of f_τ to reproduce the experimental results. On the other hand, in the right panel of figure 3, we show the variation of θ_{23} with f_e (blue dots), f_μ (green dots) and f_τ (red dots). We see from the plot that the region around maximal θ_{23} mixing angle is ruled out in this model. The reason is that while in the $L_\mu - L_\tau$ symmetric limit, the neutrino mass matrix had a $\mu - \tau$ symmetry and hence $\theta_{23} = \pi/4$ and $\theta_{13} = 0$, once the $L_\mu - L_\tau$ symmetry is spontaneously broken, θ_{23} shifts away from maximal and θ_{13} becomes non-zero, making the model consistent with the neutrino oscillations data. The plot also shows that the allowed values of mixing angle θ_{23} lie in two separate ranges between $38^\circ \lesssim \theta_{23} \lesssim 42^\circ$ (lower octant, $\theta_{23} < 45^\circ$) and $48^\circ \lesssim \theta_{23} \lesssim 51.5^\circ$ (higher octant, $\theta_{23} > 45^\circ$) for the variation of entire considered range of parameters f_i ($i = e,\ \mu,\ \tau$) from 10^{-5} GeV to 10^{-3} GeV. Therefore, we can conclude that our model is insensitive to the octant of θ_{23}.

The allowed regions for the other remaining parameters $M_{ee} - M_{\mu\tau}$ and $V_{e\mu} - V_{e\tau}$ have been shown in figure 4. The left panel of figure 4 shows the (anti)correlation between the allowed values of the parameters M_{ee} and $M_{\mu\tau}$. The neutrino oscillation data rules out the parameter region $M_{ee} \gtrsim 500\,\text{GeV}$, $M_{\mu\tau} \gtrsim 500\,\text{GeV}$ and $M_{ee} \lesssim 5\,\text{GeV}$, $M_{\mu\tau} \lesssim 5\,\text{GeV}$. In the right panel figure 4, we have shown the allowed region in the $V_{e\mu} - V_{e\tau}$ plane. In order to keep the Yukawa couplings $h_{e\mu}$ and $h_{e\tau}$ within the perturbative regime (see eq. (2.16)) we have restricted variation of both $V_{e\mu}$ and $V_{e\tau}$ upto 280 GeV. From this plot it is clearly seen that the higher values of $V_{e\mu}$ and $V_{e\tau}$ ($V_{e\mu}$, $V_{e\tau} \gtrsim 10\,\text{GeV}$) are mostly preferred by the neutrino experiments over the smaller ones.

In the left panel of figure 5, we have shown the variation of the phase ξ with respect to the parameter $M_{\mu\tau}$. Only a very narrow range of value of ξ, placed symmetrically with respect to the line $\xi = \pi$, are allowed, which reproduce the neutrino observables in the 3σ range. It is also seen from this figure that there are no points along $\xi = \pi$ line (blue

JHEP09(2016)147

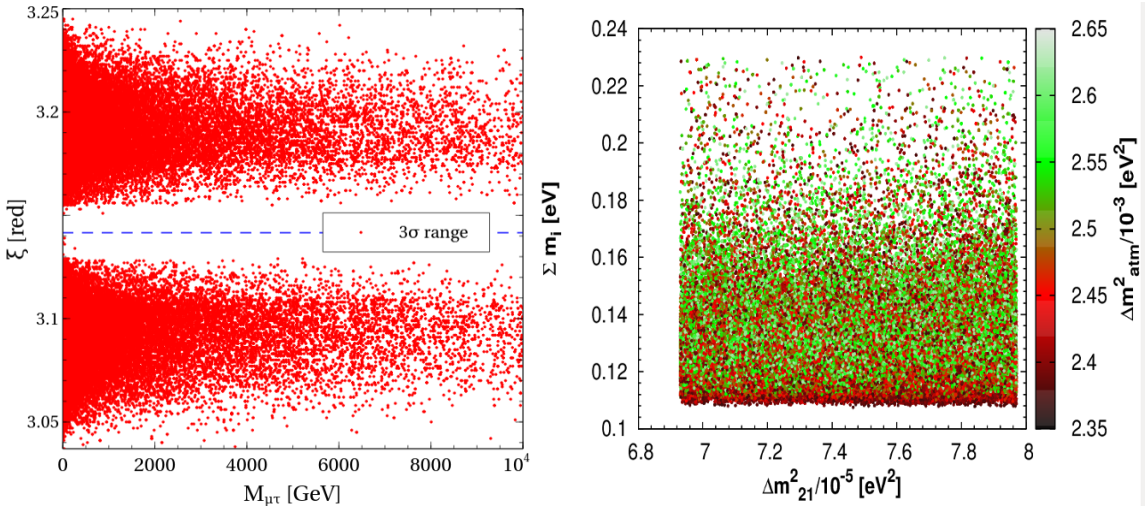

Figure 5. Left pane: allowed values of the parameters $M_{\mu\tau}$ and ξ. Blue dashed line represents $\xi = \pi$. Right panel: variation of $\sum_i m_{\nu_i}$ with the mass square differences Δm^2_{21} and Δm^2_{32}.

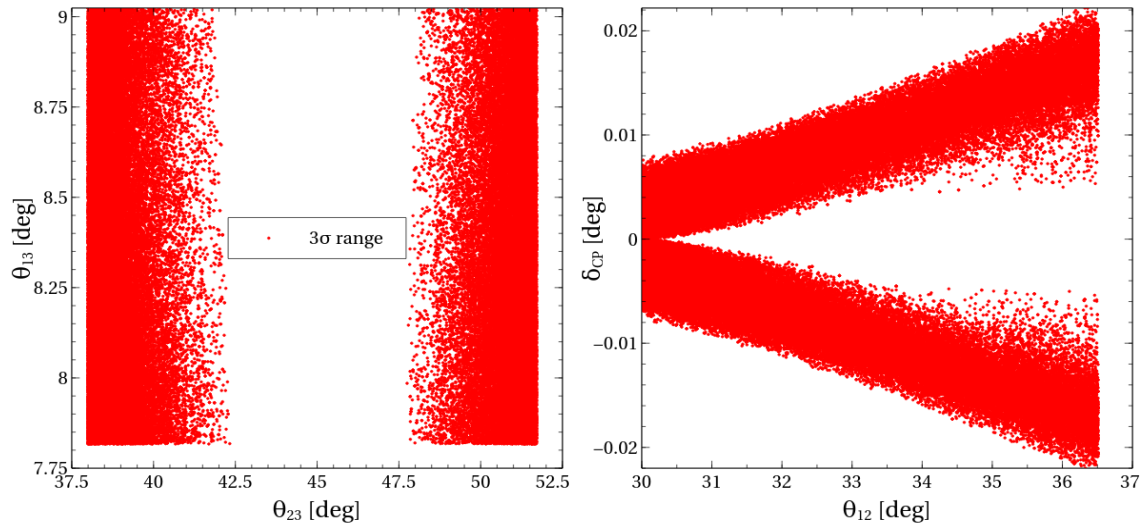

Figure 6. Left panel: variation of θ_{13} with θ_{23}. Right panel: variation of Dirac CP phase δ_{CP} with mixing angle θ_{12}.

dashed line), which indicates that for the present model, at least one element in the right handed neutrino mass matrix (here we have considered 2×3 element of M_R) has to be a complex number to satisfy the experimental results. The variation of sum of all three neutrino masses with Δm^2_{21} is presented in the right panel of figure 5. The variation of $\Delta m^2_{\rm atm}$ is also shown in the same figure. From this plot, it is evident that in this model lower values of $\sum m_i$ ($\sum m_i \leq 0.18\,\text{eV}$) are more favourable.

In the left and right panels of figure 6, we have shown the predicted ranges of the mixing angles and the Dirac CP phase. The left panel shows that for both lower and higher octant, the whole range of θ_{13} is allowed here. In the right panel of figure 6, we have plotted the

JHEP09(2016)147

predicted Dirac CP phase with respect to the mixing angle θ_{12}. We find that in our model the predicted values of Dirac CP phase are very small and symmetric around 0°. One can also note that the absolute predicted value of $|\delta_{CP}|$ increases with the mixing angle θ_{12}.

5 Dark matter

Being stable as well as electrically neutral, $\phi_{\rm DM}$ can serve as a dark matter candidate. In this section, we will compute the relic abundance of $\phi_{\rm DM}$ at the present epoch and its spin independent scattering cross section relevant for direct detection experiments. The viability of $\phi_{\rm DM}$ as a dark matter candidate will be tested by comparing its relic abundance and spin independent scattering cross section with the results obtained from Planck and LUX experiments. Finally, at the end of this section we will compute the γ-ray flux due to the annihilation of $\phi_{\rm DM}$ and compare this flux with Fermi-LAT observed γ-ray excess from the regions close to the Galactic Centre (GC).

5.1 Relic density

In the present model, since $\phi_{\rm DM}$ is a complex scalar field with a nonzero $L_\mu - L_\tau$ charge $n_{\mu\tau}$, therefore we have a non-self-conjugate DM scenario where DM particle and its antiparticle are different with respect to $n_{\mu\tau}$. In this work we assume that there is no asymmetry between the number densities of $\phi_{\rm DM}$ and $\phi^\dagger_{\rm DM}$ in the early Universe. The evolution of total DM number density n ($n = n_{\phi_{\rm DM}} + n_{\phi^\dagger_{\rm DM}}$) is governed by the well known Boltzmann equation which is given by [20]

$$\frac{dn}{dt} + 3n\mathrm{H} = -\frac{1}{2}\langle\sigma\mathrm{v}\rangle\left(n^2 - n_{eq}^2\right) , \tag{5.1}$$

where n_{eq} is the sum of equilibrium number densities of both $\phi_{\rm DM}$, $\phi^\dagger_{\rm DM}$ and H is the Hubble parameter. Moreover, $\langle\sigma\,\mathrm{v}\rangle$ is the thermally averaged annihilation cross section between $\phi_{\rm DM}$ and $\phi^\dagger_{\rm DM}$ for the processes shown in figure 7[3]. In this work, we have considered DM mass in the range 30 GeV to 500 GeV. Therefore depending on the value of $M_{\rm DM}$, $\phi_{\rm DM}$ and $\phi^\dagger_{\rm DM}$ can annihilate into the following final states: $\phi_{\rm DM}\phi^\dagger_{\rm DM} \to f\bar{f}$, W^+W^-, ZZ, $Z_{\mu\tau}Z_{\mu\tau}$, h_1h_1, h_2h_2, h_1h_2, $N_1\bar{N}_2$ and $N_1\bar{N}_3$ where f is any SM fermion. The expressions of $\langle\sigma\,\mathrm{v}\rangle$ involving actual annihilation cross section σ and modified Bessel functions is given in [20]. The factor 1/2 appearing in the right hand side of the Boltzmann equation is due to the non-self-conjugate nature of DM [20]. In terms of two dimensionless quantities Y and x the above equation can be written in the following form

$$\frac{dY}{dx} = -\left(\frac{45G}{\pi}\right)^{-\frac{1}{2}} \frac{M_{\rm DM}\sqrt{g_\star}}{x^2}\,\frac{1}{2}\langle\sigma\mathrm{v}\rangle\left(Y^2 - (Y^{eq})^2\right) , \tag{5.2}$$

where $Y = \frac{n}{\mathrm{s}}$ is the total comoving number density of $\phi_{\rm DM}$ and $\phi^\dagger_{\rm DM}$ and $x = \frac{M_{\rm DM}}{T}$ where T is the temperature of the Universe. Also, Newton's gravitational constant is denoted by

[3]We have not shown $Z_{\mu\tau}$ mediated diagrams as the coupling strength of $Z_{\mu\tau}$ with $\phi_{\rm DM}$ and $\phi^\dagger_{\rm DM}$ is proportional to $g_{\mu\tau}$ which is needed to be very small ($\sim 10^{-3}$) for the explanation of muon $(g-2)$ anomaly (see section 3).

JHEP09(2016)147

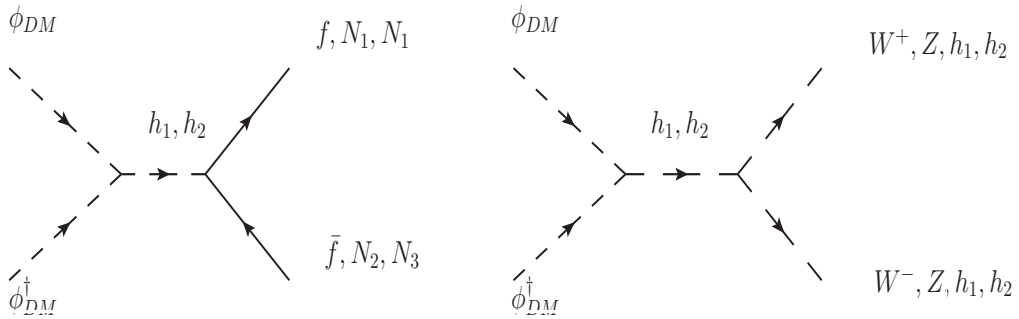

Figure 7. Feynman diagrams dominantly contributing to the annihilation cross section and hence towards the relic density of $\phi_{\rm DM}$ and $\phi^\dagger_{\rm DM}$.

G while $g_\star$ is a function of effective degrees of freedom corresponding to both energy and entropy densities of the Universe [20]. Therefore, the relic density of $\phi_{\rm DM}$ and $\phi^\dagger_{\rm DM}$ at the present epoch is given by [97, 98]

$$\Omega_{\rm DM}h^2 = 2.755 \times 10^8 \left(\frac{M_{\rm DM}}{\rm GeV}\right) Y(T_0)\,. \tag{5.3}$$

$Y(T_0)$ is the total comoving number density of $\phi_{\rm DM}$ and $\phi^\dagger_{\rm DM}$ for the present temperature of the Universe ($T_0 \sim 10^{-13}\,$GeV), which can be obtained by solving eq. (5.2).

5.2 Direct detection

Dark matter direct detection experiments use the principle of elastic scattering between dark matter particles and detector nuclei. If DM particles scatter off the detector nuclei elastically then the information about the nature of DM particles and their interaction type with SM particles (quarks) can be obtained by measuring the recoil energy of the nuclei. Since the DM particles are nonrelativistic (cold dark matter), therefore the energy deposited to the nuclei are extremely small ($\sim$ keV range). Hence in order to measure it accurately, low background as well as low threshold detector is required. In the present model, the elastic scattering of both $\phi_{\rm DM}$ and $\phi^\dagger_{\rm DM}$ can occur only through the exchange of scalar bosons h_1, h_2. Unlike the other U(1) extensions of the SM where the extra neutral gauge bosons can interact with the quarks (such as U(1)$_{B-L}$ model [92]), here $Z_{\mu\tau}$ does not couple with the quark sector and consequently, the spin independent scattering cross sections of the DM particle and its antiparticle are equal. The expression of spin independent scattering cross section of DM with nucleon (N) is given by

$$\sigma_{\rm SI} = \frac{\mu^2}{4\pi}\left[\frac{M_N\, f_N\, \cos\alpha}{M_{\rm DM}\, v}\left(\frac{\tan\alpha\, g_{\phi_{\rm DM}\phi^\dagger_{\rm DM}h_2}}{M^2_{h_2}} - \frac{g_{\phi_{\rm DM}\phi^\dagger_{\rm DM}h_1}}{M^2_{h_1}}\right)\right]^2, \tag{5.4}$$

where μ is the reduced mass between DM and N while $f_N \sim 0.3$ [99] is the nuclear form factor. $g_{\phi_{\rm DM}\phi^\dagger_{\rm DM}h_i}$ is the vertex factor involving fields $\phi_{\rm DM}$, $\phi^\dagger_{\rm DM}$ and h_i ($i = 1, 2$) and its expression is given in table 3.

JHEP09(2016)147

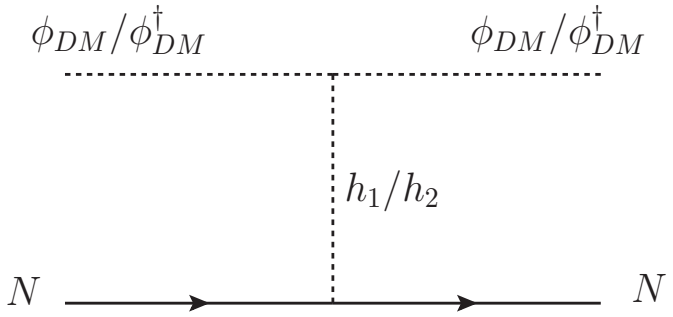

Figure 8. Feynman diagram for the elastic scattering of $\phi_{\rm DM}$ and $\phi^{\dagger}_{\rm DM}$ with detector nucleon (N).

Vertex $a\,b\,c$	Vertex Factor g_{abc}
$q\,\bar{q}\,h_1$	$-\frac{M_q}{v}\cos\alpha$
$q\,\bar{q}\,h_2$	$\frac{M_q}{v}\sin\alpha$
$W^+\,W^-\,h_1$	$\frac{2\,M_W^2\cos\alpha}{v}$
$W^+\,W^-\,h_2$	$-\frac{2\,M_W^2\sin\alpha}{v}$
$Z\,Z\,h_1$	$\frac{2\,M_Z^2\cos\alpha}{v}$
$Z\,Z\,h_2$	$-\frac{2\,M_Z^2\sin\alpha}{v}$
$N_e\,N_\mu\,(N_\tau)\,h_1$	$\sqrt{2}\sin\alpha\,h_{e\mu}\,(h_{e\tau})$
$N_e\,N_\mu\,(N_\tau)\,h_2$	$\sqrt{2}\cos\alpha\,h_{e\mu}\,(h_{e\tau})$
$l\,\bar{l}\,h_1$	$-\frac{M_l}{v}\cos\alpha$
$l\,\bar{l}\,h_2$	$\frac{M_l}{v}\sin\alpha$
$l\,\bar{l}\,Z_{\mu\tau}$	$\pm g_{\mu\tau}\,\gamma^{\rho}(+\text{ for }\mu,-\text{ for }\tau)$
$\phi_{\rm DM}\,\phi^{\dagger}_{\rm DM}\,h_1$	$-(v\,\lambda_{Dh}\cos\alpha+v_{\mu\tau}\lambda_{DH}\sin\alpha)$
$\phi_{\rm DM}\,\phi^{\dagger}_{\rm DM}\,h_2$	$(v\,\lambda_{Dh}\sin\alpha-v_{\mu\tau}\,\lambda_{DH}\cos\alpha)$
$\phi_{\rm DM}\,\phi^{\dagger}_{\rm DM}\,Z_{\mu\tau}$	$n_{\mu\tau}\,g_{\mu\tau}\,(p_2-p_1)^{\rho}$
$\phi_{\rm DM}\,\phi^{\dagger}_{\rm DM}\,h_1\,h_1$	$-(\lambda_{Dh}\,\cos^2\alpha+\lambda_{DH}\,\sin^2\alpha)$
$\phi_{\rm DM}\,\phi^{\dagger}_{\rm DM}\,h_2\,h_2$	$-(\lambda_{Dh}\,\sin^2\alpha+\lambda_{DH}\,\cos^2\alpha)$
$\phi_{\rm DM}\,\phi^{\dagger}_{\rm DM}\,h_1\,h_2$	$\sin\alpha\cos\alpha(\lambda_{Dh}-\lambda_{DH})$
$\phi_{\rm DM}\,\phi^{\dagger}_{\rm DM}\,Z_{\mu\tau}\,Z_{\mu\tau}$	$2\,g^2_{\mu\tau}n^2_{\mu\tau}$
$\phi_{\rm DM}\,\phi^{\dagger}_{\rm DM}\phi_{\rm DM}\,\phi^{\dagger}_{\rm DM}$	$-4\,\lambda_{\rm DM}$

Table 3. All relevant vertex factors required for the computation of DM annihilation as well as scattering cross sections.

JHEP09(2016)147

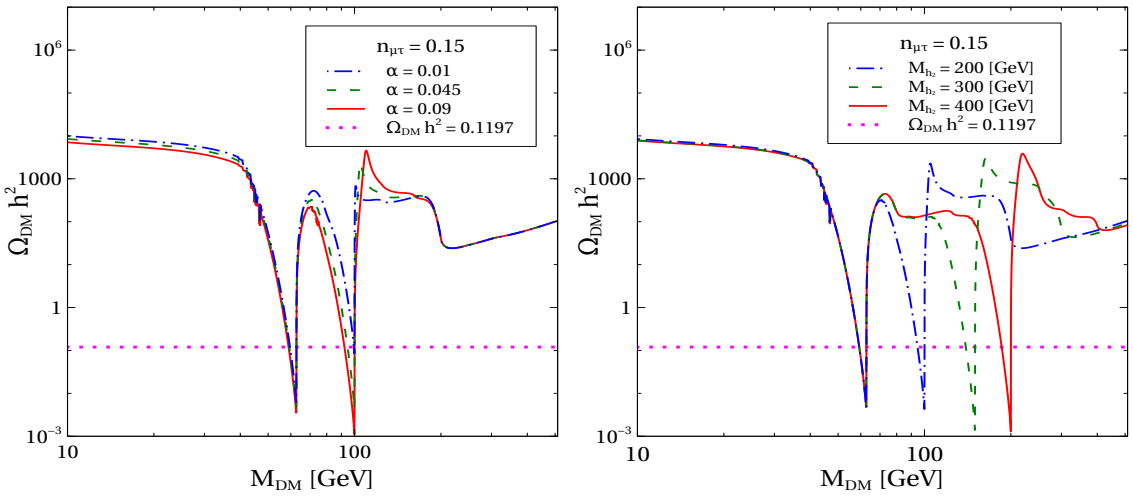

Figure 9. Left (Right) Panel: variation of relic density $\Omega_{\rm DM}h^2$ with respect to the DM mass $M_{\rm DM}$ for three different value of mixing angle α (M_{h_2}), while other the values of parameters have been kept fixed at $\lambda_{DH} = 0.01$, $\lambda_{Dh} = 0.001$, and $M_{h_2} = 200\,\text{GeV}$ ($\alpha = 0.045$ rad).

5.3 Results

We have computed the relic density of DM using micrOMEGAs [100] package and the implementation of the present model in micrOMEGAS has been done using the LanHEP [101] package. For the relic density calculation, we have considered the following benchmark values of the parameters related to the neutrino sector,

- Masses of the three heavy neutrinos: $M_{N_1} = 332.88\,\text{GeV}$, $M_{N_2} = 279.06\,\text{GeV}$ and $M_{N_3} = 168.28\,\text{GeV}$,
- Yukawa couplings: $h_{e\mu} = 2.44$ and $h_{e\tau} = 1.28$.

We have checked that these adopted values of right handed neutrino masses and Yukawa couplings reproduce all the experimentally measurable quantities of the neutrino sector within their 1σ range [12]. Moreover like the previous section, here also we have used our benchmark point $M_{Z_{\mu\tau}} = 100\,\text{MeV}$ and $g_{\mu\tau} = 9 \times 10^{-4}$, which are required to explain the muon $(g-2)$ anomaly.

In the left panel of figure 9, we show the variation of the DM relic density with its mass for three different values of the scalar mixing angle, $\alpha = 0.01$ rad, 0.045 rad and 0.09 rad[4] respectively. From this plot it is clearly seen that DM relic density satisfies the central value of Planck limit ($\Omega_{\rm DM}h^2 = 0.1197$) only around the two resonance regions where the mass of DM is nearly equal to half of the mediator mass i.e. $M_{\rm DM} \sim M_{h_i}/2$ ($i = 1, 2$). Therefore the first resonance occurs when DM mass is around 62 GeV and it is due to the SM-like Higgs boson h_1 while the second one is due to extra Higgs boson h_2 of mass 200 GeV. Like the left panel of figure 9, the right panel also shows the variation of $\Omega_{\rm DM}h^2$

[4]We have checked that these values of mixing angle α are allowed by the LHC results on Higgs signal strength [74] and invisible decay width [102].

JHEP09(2016)147

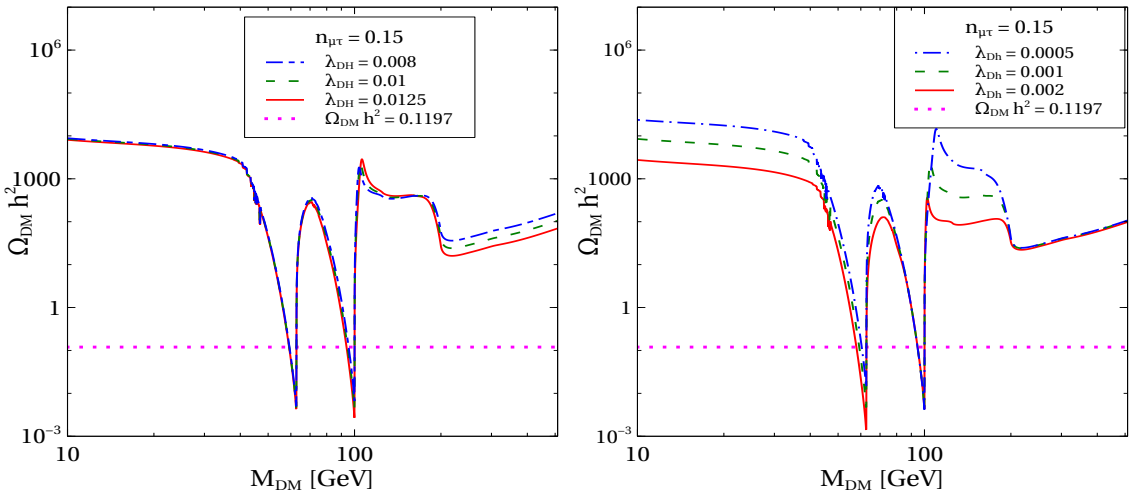

Figure 10. Left (Right) Panel: variation of relic density Ωh^2 with respect to the mass of the dark matter $M_{\rm DM}$ for three different value of λ_{DH} (λ_{Dh}), while other parameters value are kept fixed at $M_{h_2} = 200\,\text{GeV}$, $\alpha = 0.045$ rad and $\lambda_{Dh} = 0.001$ ($\lambda_{DH} = 0.01$).

with $M_{\rm DM}$ but in this case three different plots are generated for three different values of $M_{h_2} = 200\,\text{GeV}$ (blue dashed dot line), 300 GeV (green dashed line) and 400 GeV (red solid line), respectively. Similar to the left panel, here also the DM relic density satisfies the Planck limit only around the resonance regions. However in this plot, as we have varied the mass of h_2, therefore instead of getting a single resonance region for h_2 (as in the left panel) we have found three resonance regions at $M_{\rm DM} \sim 100\,\text{GeV}$, 150 GeV and 200 GeV for $M_{h_2} = 200\,\text{GeV}$, 300 GeV and 400 GeV, respectively. For all three cases the resonance due to the SM-like Higgs boson h_1 occurs at the same value of $M_{\rm DM} \sim 62.5\,\text{GeV}$ as we have fixed the mass of h_1 at 125.5 GeV. Plots in both panels are generated for $n_{\mu\tau} = 0.15$.

Left and right panels of figure 10 represent the variation of relic density $\Omega_{\rm DM}h^2$ with the dark matter mass $\phi_{\rm DM}$ for there different values of parameter λ_{DH} and λ_{Dh}, respectively. These plots also show the appearance of two resonance regions due to the two mediating scalar bosons. However, from this figure one can notice the effect of parameters λ_{Dh} and λ_{DH} on the DM relic density with respect to the variation of $M_{\rm DM}$. In the low mass region ($M_{\rm DM} \lesssim 80\,\text{GeV}$), SM-like Higgs boson mediated diagrams dominantly contribute to the pair annihilation processes of $\phi_{\rm DM}$ and $\phi^\dagger_{\rm DM}$ while the contribution of extra Higgs mediated diagrams become superior for the high DM mass region ($M_{\rm DM} \gtrsim 80\,\text{GeV}$). From the expression of $\phi_{\rm DM}\,\phi^\dagger_{\rm DM}\,h_1$ vertex factor given in table 3, one can see that the effect of the parameter λ_{DH} on $\langle\sigma v\rangle$ is mixing angle suppressed (i.e. multiplied by $\sin\alpha$). Therefore, in the left panel for low DM mass region the effect of λ_{DH} to $\Omega_{\rm DM}h^2$ is small. On the other hand, in the expression of vertex factor of $\phi_{\rm DM}\,\phi^\dagger_{\rm DM}\,h_1$, the parameter λ_{Dh} appears with $\cos\alpha$ and hence we see a considerable effect of λ_{Dh} on $\Omega_{\rm DM}h^2$ in the right panel (low DM mass region). For the extreme right region of both panels ($M_{\rm DM} \gtrsim 200\,\text{GeV}$), the dominant pair annihilation channel is $\phi_{\rm DM}\phi^\dagger_{\rm DM} \to h_2 h_2$. Hence, the impact of λ_{DH} and λ_{Dh} to $\Omega_{\rm DM}h^2$ can well be understood from the expression of $\phi_{\rm DM}\phi^\dagger_{\rm DM}h_2h_2$ vertex factor (see

JHEP09(2016)147

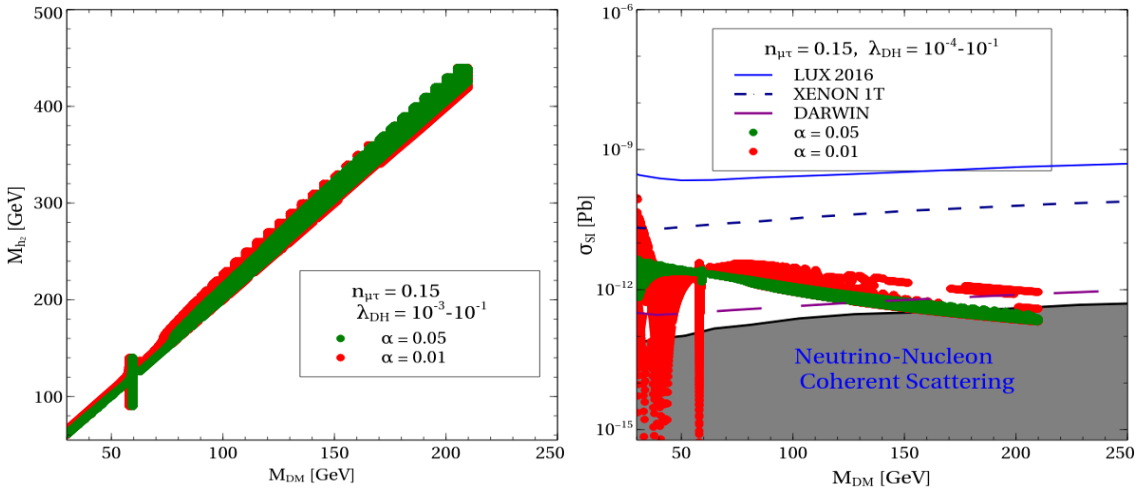

Figure 11. Left Panel: allowed values of M_{h_2} with respect to the variation of the dark matter mass $M_{\rm DM}$ for two different value of mixing angle α. Right panel: variation of spin independent scattering cross sections of dark matter with its mass. All the points in both plots satisfy the Planck limit on DM relic density in 1σ range ($\Omega_{\rm DM}h^2 = 0.1197 \pm 0.0022$ [18]) and these two plots are generated for $\lambda_{Dh} = 0.001$.

table 3). In the intermediate region ($80\,\text{GeV} < M_{\rm DM} < 200\,\text{GeV}$), $\phi_{\rm DM}\phi^\dagger_{\rm DM} \to W^+W^-$, ZZ and h_1h_1 channels mainly contribute to DM relic density and in the right panel for $100\,\text{GeV} < M_{\rm DM} < 200\,\text{GeV}$, the variation of $\Omega_{\rm DM}h^2$ with respect to λ_{Dh} resulting from DM pair annihilation into h_1h_1 final state.

In the left panel of figure 11, we show the allowed values of M_{h_2} which reproduce the correct DM relic density for the variation of $M_{\rm DM}$ in the range 30 GeV to 500 GeV. In this plot we have varied the mass of extra Higgs boson M_{h_2} in the range 60 GeV to 450 GeV and λ_{DH} from 0.001 to 0.1. From this plot it is evident that for a particular value of dark matter mass the corresponding allowed values of M_{h_2} lie around $2\,M_{\rm DM}$. The reason behind this nature is that the relic abundance of dark matter (both $\phi_{\rm DM}$ and $\phi^\dagger_{\rm DM}$) satisfies the observed DM density only around the resonance regions (when mediator mass $M_{h_i} \sim 2{\times}M_{\rm DM}$, $i = 1, 2$ see figure 9 and figure 10). The allowed range of M_{h_2} for a particular DM mass does not vary much for the change of mixing angle α from 0.01 rad (red coloured region) to 0.05 rad (green colour region). Moreover, we restrict M_{h_2} upto 430 GeV to remain within the perturbative regime ($\lambda_H < 4\,\pi$) and hence the relic density condition is not satisfied beyond $M_{\rm DM} = 215$ GeV Furthermore, near $M_{\rm DM} \sim 60$ GeV, one can see that a broad range of M_{h_2} values are allowed, which indicates that in this region the SM-like Higgs contributes dominantly giving the wide range of M_{h_2} values for which the DM relic density is satisfied. Spin independent elastic scattering cross section ($\sigma_{\rm SI}$) of DM with with its mass has been plotted in the the right panel of figure 11 for two different values of $\alpha = 0.01$ rad (green coloured region) and 0.05 rad (red coloured region) respectively. This plot is also generated for $60\,\text{GeV} \leq M_{h_2} \leq 430\,\text{GeV}$, $0.001 \leq \lambda_{DH} \leq 0.1$ and $\lambda_{Dh} = 0.001$ and all the points within the red and green coloured patch satisfy the Planck result. For comparison with current experimental limits on $\sigma^{\rm SI}$ from DM direct detection experiments we have plotted the result of

JHEP09(2016)147

LUX-2016 (blue solid line) in the same figure. Moreover, we have also shown the predicted results from the "ton-scale" direct detection experiments like XENON 1T [23] (blue dashed line) and DARWIN [103] (long dashed purple line). From this figure it is evident that the validity of our model can be explored in near future by these "ton-scale" experiments.

5.4 Indirect detection: Fermi-LAT γ-ray excess from the galactic centre

Over the past few years, the existence of an unidentified excess of γ-rays with energy 1-3 GeV from the direction of the Galactic Centre has been reported by several groups [30, 104–114] after analysing the Fermi-LAT publicly available data [27]. There are some astrophysical explanations such as unresolved point sources (e.g. millisecond pulsar) around the GC which may be responsible for this anomalous gamma-ray excess [28, 29]. However, the spectrum and morphology of this gamma-ray excess is also very similar to that expected from the annihilation [115] or decay (see [116] and references therein) of dark matter in the GC. In terms of an annihilating DM scenario this excess can be well explained by a dark matter of mass around $48.7^{+6.4}_{-5.2}$ GeV and with an annihilation cross section $\langle\sigma \mathrm{v}_{b\bar{b}}\rangle = 1.75^{+0.28}_{-0.26} \times 10^{-26}$ cm^3/s into $b\bar{b}$ final state [30]. Thereafter these b quarks produce excess γ-ray from their hadronization processes. The above quantities $M_{\rm DM}$ and $\langle\sigma \mathrm{v}_{b\bar{b}}\rangle$ depend on the specific choice of dark matter halo profile. In ref. [30] authors have used an NFW halo profile [117] with index $\gamma = 1.26$, $r_s = 20$ kpc, local dark matter density $\rho_\odot = 0.4\,\mathrm{GeV/cm^3}$ and a region of interest (ROI) around GC where galactic latitude b, longitude l vary in the range $2^0 < |b| < 20^0$, $|l| < 20^0$ respectively during the analysis of Fermi-LAT data. Since our knowledge about the exact values of DM halo profile parameters such as γ and $\rho_\odot$ is limited, there are some uncertainties in these profile parameters and this can affect the calculated value of $\langle\sigma \mathrm{v}_{b\bar{b}}\rangle$. Due to this uncertainty the allowed values of annihilation cross section for the $b\bar{b}$ channel can vary in the range $\mathcal{A}\times$ the best fit value of $\langle\sigma \mathrm{v}_{b\bar{b}}\rangle$ which is $1.75 \times 10^{-26}\,\mathrm{cm^3/s}$ while $\mathcal{A}$ can be any number between 0.17 to 5.3 [30]. For $\gamma = 1.26$, $\rho_\odot = 0.4\,\mathrm{GeV/cm^3}$ and $r_s = 20$ kpc. For the value of $\mathcal{A} = 1$, we have found that, in the present $L_\mu - L_\tau$ symmetric model with a DM candidate $\phi_{\rm DM}$ such explanation of this anomalous gamma-excess is indeed possible from the pair annihilation of $\phi_{\rm DM}$ and $\phi^\dagger_{\rm DM}$ at the Galactic Centre. In our earlier work [92] we have done a detailed computation of γ-ray flux resulting from the annihilation of a complex scalar dark matter at the GC. Therefore, the process of computing gamma-ray flux from the pair annihilation of $\phi_{\rm DM}$ and $\phi^\dagger_{\rm DM}$ for the present scenario is very similar to that work and hence these intermediated steps are not repeated here. Note that since we are dealing with non-self-conjugate dark matter, therefore, there will be an extra half factor in the expression for the differential gamma-ray flux [92, 118]. Hence in our case, the best fit value of $\langle\sigma \mathrm{v}_{b\bar{b}}\rangle$ will be $3.50 \times 10^{-26}\,\mathrm{cm^3/s}$. Following the same procedure given in [92] we have found that, for the present model, the excess gamma-rays flux observed by Fermi-LAT can be reproduced for an annihilating dark matter of mass $M_{\rm DM} = 52\,\mathrm{GeV}$ and $\langle\sigma \mathrm{v}_{b\bar{b}}\rangle = 3.856 \times 10^{-26}\,\mathrm{cm^3/s}$. In this case, DM annihilation to $b\bar{b}$ channel dominantly occurs through the resonance of extra Higgs boson (h_2) with resonating mass $M_{h_2} = 104.025\,\mathrm{GeV}$ and coupling parameters $\lambda_{DH} = 0.01$, $\lambda_{Dh} = 0.001$ and scalar mixing angle $\alpha = 0.045$ rad.

JHEP09(2016)147

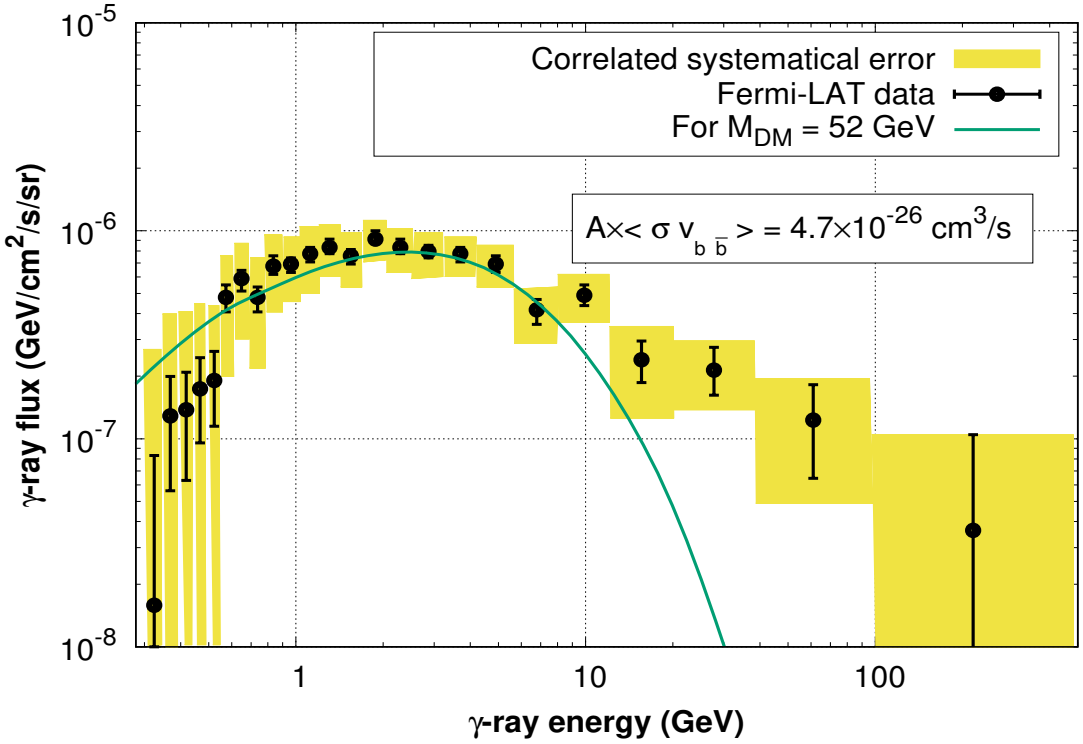

Figure 12. Gamma-ray flux obtained from the pair annihilation of $\phi_{\rm DM}$ and $\phi^{\dagger}_{\rm DM}$ at the Galactic Centre for $M_{\rm DM} = 52\,\text{GeV}$, $\langle\sigma \text{v}_{b\bar{b}}\rangle = 3.856 \times 10^{-26}\,\text{cm}^3/\text{s}$ and $\mathcal{A} = 1.219$.

In figure 12, green solid line represents the γ-ray flux that we have computed for a $M_{\rm DM} = 52\,\text{GeV}$ while the value of $b\bar{b}$ annihilation cross section is $3.856 \times 10^{-26}\,\text{cm}^3/\text{s}$. The correlated systematic errors are represented by the yellow boxes while the Fermi-LAT uncorrelated statistical uncertainties are shown by the black error bars taken from [119]. We have found that in order to reproduced the Fermi-LAT observed γ-ray flux for a 52 GeV non-self-conjugate DM, the quantity $\mathcal{A} \times \langle\sigma \text{v}_{b\bar{b}}\rangle$ must be $4.7 \times 10^{-26}\,\text{cm}^3/\text{s}$ [92]. This requires DM halo profile error parameter $\mathcal{A}$ to be ~ 1.22, well inside its allowed range between 0.17 to 5.3 [30].

6 Summary and conclusion

Although Standard Model (SM) is a well established theory of elementary particle physics, it cannot explain the muon $(g-2)$ anomaly, the small neutrino masses and peculiar mixing pattern, and the existence of Dark Matter (DM). Therefore, the SM has to be extended to explain these observational evidences. In the present work we have extended the SM gauge group $\text{SU}(3)\times\text{SU}(2)_L\times\text{U}(1)_Y$ by a local $\text{U}(1)_{L_\mu - L_\tau}$ gauge group. Since we require $\text{U}(1)_{L_\mu - L_\tau}$ to be local, we get an extra gauge boson, $Z_{\mu\tau}$. One of the most appealing aspects of the gauged $\text{U}(1)_{L_\mu - L_\tau}$ extension of the SM is that it does not introduce any anomaly in the theory [37–39]. We introduce a scalar with non-trivial $L_\mu - L_\tau$ number which picks up a VEV, breaking the $\text{U}(1)_{L_\mu - L_\tau}$ symmetry spontaneously and making $Z_{\mu\tau}$ massive. This

JHEP09(2016)147

extra massive $Z_{\mu\tau}$ provides additional contributions to the magnetic moment of the muon, which can explain the observed data on muon $(g-2)$ for $Z_{\mu\tau}$ of $\mathcal{O}$ (100 MeV) and low values of gauge coupling $g_{\mu\tau} \lesssim 10^{-3}$. We fixed the value of $g_{\mu\tau}$ and $M_{Z_{\mu\tau}}$ such that they are allowed by the neutrino trident process [73] and calculated the muon $(g-2)$ to within $3.2\,\sigma$ of the measured value. We kept $g_{\mu\tau}$ and $M_{Z_{\mu\tau}}$ fixed at these values throughout the rest of the paper.

The $L_\mu - L_\tau$ symmetry, being also a flavor symmetry, provides a natural way of explaining the peculiar mixing pattern of the light neutrinos. We added to the particle content, three right-handed neutrinos (N_e, N_μ, N_τ) and generated small neutrino masses naturally through the canonical Type-I seesaw mechanism. The N_e, N_μ, N_τ are given $L_\mu - L_\tau$ flavor numbers, making the right-handed neutrino mass matrix and as a result the light Majorana neutrino mass matrix $\mu - \tau$ symmetric. This leads to $\theta_{23} = \pi/4$ and $\theta_{13} = 0$, inconsistent with the neutrino oscillation data. However, when the $L_\mu - L_\tau$ symmetry gets spontaneously broken, it generates additional terms in the right-handed and consequently light neutrino mass matrix giving a good explanation of the global neutrino oscillation data. We scanned the five-dimensional model parameter space of our model and found the regions of this space that are consistent with the allowed neutrino oscillation parameters within their 3σ ranges. We discussed the correlations between the model parameters. We also presented the oscillation parameters predicted by our model. In particular, we showed that our model can explain the observed value of θ_{13} very naturally, predicts a value of θ_{23} that is not maximal, does not distinguish between the two octants of θ_{23} and predicts the Dirac δ_{CP} phase to be very close to 0. Hence our model predicts that no discernible CP violation will be observed in the long baseline experiments.

We next introduced another complex scalar $\phi_{\rm DM}$ which does not take a VEV and hence is a good candidate for DM. The stability of this complex scalar is ensured by giving it a suitable $L_\mu - L_\tau$ charge, making it impossible to write any decay terms in the Lagrangian, even after the $L_\mu - L_\tau$ symmetry is broken spontaneously. We showed that due to the very small gauge coupling $g_{\mu\tau}$ required to explain the anomalous muon $(g-2)$ data, the $Z_{\mu\tau}$-portal diagrams do not contribute to the DM phenomenology. The relic abundance and signature of our model in direct and indirect experiments come through the Higgs portal. We calculated the relic abundance of DM in this model and showed that the observational constraints from Plank can be satisfied for the two resonance regions corresponding to the scenario where $M_{\rm DM} \simeq M_{h_1}/2$ and $M_{\rm DM} \simeq M_{h_2}/2$, respectively, where M_{h_1} and M_{h_2} are the masses of h_1 and h_2, the two Higgs scalars in our model. We presented the prediction of our model in forthcoming direct detection experiments and showed that for a wide range of model parameter space, XENON 1T and DARWIN could see a positive signal for $\phi_{\rm DM}$. Likewise, they can constrain large parts of the model parameter in case they do not observe any WIMP signal. We also showed that for $\phi_{\rm DM} \simeq 52\,\text{GeV}$, our model can explain the galactic centre gamma ray excess in the $1-3\,\text{GeV}$ range observed by FermiLAT.

In conclusion, we propose a gauged $L_\mu - L_\tau$ extension of the SM with two additional scalars and three additional right-handed neutrinos. This model can explain the anomalous muon $(g-2)$ data, small neutrino masses and peculiar mixing pattern, and provides a viable dark matter candidate. It can explain the relic abundance as well as the galactic centre

JHEP09(2016)147

gamma ray excess while satisfying all other experimental bounds. It also predict no CP violation in neutrino oscillation experiments. This model is phenomenologically rich and predictive and should be testable in forthcoming high energy physics experiments, including collider experiments, dark matter experiments as well as neutrino oscillation experiments.

Acknowledgments

One of the authors A.B. wants to thank Mainak Chakraborty for some valuable discussions. A.B. also likes to thank Arindam Mazumdar for his help in gnuplot. The authors would like to thank the Department of Atomic Energy (DAE) Neutrino Project under the XII plan of Harish-Chandra Research Institute. SK and AB also acknowledge the cluster computing facility at HRI (http://cluster.hri.res.in). This project has received funding from the European Union's Horizon 2020 research and innovation programme InvisiblesPlus RISE under the Marie Skłodowska-Curie grant agreement No 690575. This project has received funding from the European Union's Horizon 2020 research and innovation programme Elusives ITN under the Marie Skłodowska-Curie grant agreement No 674896.

References

[1] C.L. Cowan, F. Reines, F.B. Harrison, H.W. Kruse and A.D. McGuire, *Detection of the free neutrino: a confirmation*, *Science* **124** (1956) 103 [INSPIRE].

[2] SUPER-KAMIOKANDE collaboration, Y. Fukuda et al., *Evidence for oscillation of atmospheric neutrinos*, *Phys. Rev. Lett.* **81** (1998) 1562 [hep-ex/9807003] [INSPIRE].

[3] SNO collaboration, Q.R. Ahmad et al., *Direct evidence for neutrino flavor transformation from neutral current interactions in the Sudbury Neutrino Observatory*, *Phys. Rev. Lett.* **89** (2002) 011301 [nucl-ex/0204008] [INSPIRE].

[4] KAMLAND collaboration, K. Eguchi et al., *First results from KamLAND: evidence for reactor anti-neutrino disappearance*, *Phys. Rev. Lett.* **90** (2003) 021802 [hep-ex/0212021] [INSPIRE].

[5] DAYA BAY collaboration, F.P. An et al., *Measurement of the reactor antineutrino flux and spectrum at Daya Bay*, *Phys. Rev. Lett.* **116** (2016) 061801 [arXiv:1508.04233] [INSPIRE].

[6] RENO collaboration, J.H. Choi et al., *Observation of energy and baseline dependent reactor antineutrino disappearance in the RENO experiment*, *Phys. Rev. Lett.* **116** (2016) 211801 [arXiv:1511.05849] [INSPIRE].

[7] DOUBLE CHOOZ collaboration, Y. Abe et al., *Improved measurements of the neutrino mixing angle θ_{13} with the Double CHOOZ detector*, *JHEP* **10** (2014) 086 [*Erratum ibid.* **02** (2015) 074] [arXiv:1406.7763] [INSPIRE].

[8] T2K collaboration, K. Abe et al., *Measurements of neutrino oscillation in appearance and disappearance channels by the T2K experiment with 6.6×10^{20} protons on target*, *Phys. Rev.* **D 91** (2015) 072010 [arXiv:1502.01550] [INSPIRE].

JHEP09(2016)147

[9] T2K collaboration, M. Ravonel Salzgeber, *Anti-neutrino oscillations with T2K*, arXiv:1508.06153 [INSPIRE].

[10] NOvA collaboration, P. Adamson et al., *First measurement of electron neutrino appearance in NOvA*, *Phys. Rev. Lett.* **116** (2016) 151806 [arXiv:1601.05022] [INSPIRE].

[11] NOvA collaboration, P. Adamson et al., *First measurement of muon-neutrino disappearance in NOvA*, *Phys. Rev.* **D 93** (2016) 051104 [arXiv:1601.05037] [INSPIRE].

[12] F. Capozzi, E. Lisi, A. Marrone, D. Montanino and A. Palazzo, *Neutrino masses and mixings: status of known and unknown* 3ν *parameters*, *Nucl. Phys.* **B 908** (2016) 218 [arXiv:1601.07777] [INSPIRE].

[13] Y. Sofue and V. Rubin, *Rotation curves of spiral galaxies*, *Ann. Rev. Astron. Astrophys.* **39** (2001) 137 [astro-ph/0010594] [INSPIRE].

[14] D. Clowe, A. Gonzalez and M. Markevitch, *Weak lensing mass reconstruction of the interacting cluster* 1*E*0657-558*: direct evidence for the existence of dark matter*, *Astrophys. J.* **604** (2004) 596 [astro-ph/0312273] [INSPIRE].

[15] D. Harvey, R. Massey, T. Kitching, A. Taylor and E. Tittley, *The non-gravitational interactions of dark matter in colliding galaxy clusters*, *Science* **347** (2015) 1462 [arXiv:1503.07675] [INSPIRE].

[16] M. Bartelmann and P. Schneider, *Weak gravitational lensing*, *Phys. Rept.* **340** (2001) 291 [astro-ph/9912508] [INSPIRE].

[17] WMAP collaboration, G. Hinshaw et al., *Nine-year Wilkinson Microwave Anisotropy Probe (WMAP) observations: cosmological parameter results*, *Astrophys. J. Suppl.* **208** (2013) 19 [arXiv:1212.5226] [INSPIRE].

[18] PLANCK collaboration, P.A.R. Ade et al., *Planck* 2015 *results. XIII. Cosmological parameters*, arXiv:1502.01589 [INSPIRE].

[19] E.J. Copeland, M. Sami and S. Tsujikawa, *Dynamics of dark energy*, *Int. J. Mod. Phys.* **D 15** (2006) 1753 [hep-th/0603057] [INSPIRE].

[20] P. Gondolo and G. Gelmini, *Cosmic abundances of stable particles: improved analysis*, *Nucl. Phys.* **B 360** (1991) 145 [INSPIRE].

[21] M. Srednicki, R. Watkins and K.A. Olive, *Calculations of relic densities in the early universe*, *Nucl. Phys.* **B 310** (1988) 693 [INSPIRE].

[22] LUX collaboration, D.S. Akerib et al., *Improved limits on scattering of weakly interacting massive particles from reanalysis of* 2013 *LUX data*, *Phys. Rev. Lett.* **116** (2016) 161301 [arXiv:1512.03506] [INSPIRE].

[23] XENON collaboration, E. Aprile et al., *Physics reach of the XENON*1*T dark matter experiment*, *JCAP* **04** (2016) 027 [arXiv:1512.07501] [INSPIRE].

[24] SUPERCDMS collaboration, R. Agnese et al., *Search for low-mass weakly interacting massive particles with SuperCDMS*, *Phys. Rev. Lett.* **112** (2014) 241302 [arXiv:1402.7137] [INSPIRE].

[25] LUX collaboration, A. Manalaysay, *Dark-matter results from* 332 *new live days of LUX data*, talk at *Identification of Dark Matter*, https://idm2016.shef.ac.uk/indico/event/0/contribution/50/material/slides/0.pdf, The University of Sheffield, Sheffield U.K. July 21 2016.

JHEP09(2016)147

[26] D. Hooper, *Particle dark matter*, arXiv:0901.4090 [INSPIRE].

[27] FERMI-LAT collaboration, W.B. Atwood et al., *The Large Area Telescope on the Fermi gamma-ray space telescope mission*, *Astrophys. J.* **697** (2009) 1071 [arXiv:0902.1089] [INSPIRE].

[28] S.K. Lee, M. Lisanti, B.R. Safdi, T.R. Slatyer and W. Xue, *Evidence for unresolved γ-ray point sources in the inner galaxy*, *Phys. Rev. Lett.* **116** (2016) 051103 [arXiv:1506.05124] [INSPIRE].

[29] R. Bartels, S. Krishnamurthy and C. Weniger, *Strong support for the millisecond pulsar origin of the galactic center GeV excess*, *Phys. Rev. Lett.* **116** (2016) 051102 [arXiv:1506.05104] [INSPIRE].

[30] F. Calore, I. Cholis, C. McCabe and C. Weniger, *A tale of tails: dark matter interpretations of the Fermi GeV excess in light of background model systematics*, *Phys. Rev.* **D 91** (2015) 063003 [arXiv:1411.4647] [INSPIRE].

[31] S.L. Adler, *Axial vector vertex in spinor electrodynamics*, *Phys. Rev.* **177** (1969) 2426 [INSPIRE].

[32] W.A. Bardeen, *Anomalous Ward identities in spinor field theories*, *Phys. Rev.* **184** (1969) 1848 [INSPIRE].

[33] R. Delbourgo and A. Salam, *The gravitational correction to PCAC*, *Phys. Lett.* **B 40** (1972) 381 [INSPIRE].

[34] T. Eguchi and P.G.O. Freund, *Quantum gravity and world topology*, *Phys. Rev. Lett.* **37** (1976) 1251 [INSPIRE].

[35] N. Okada and O. Seto, *Higgs portal dark matter in the minimal gauged $\mathrm{U}(1)_{B-L}$ model*, *Phys. Rev.* **D 82** (2010) 023507 [arXiv:1002.2525] [INSPIRE].

[36] S. Patra, W. Rodejohann and C.E. Yaguna, *A new B-L model without right-handed neutrinos*, arXiv:1607.04029 [INSPIRE].

[37] X.G. He, G.C. Joshi, H. Lew and R.R. Volkas, *New Z' phenomenology*, *Phys. Rev.* **D 43** (1991) 22 [INSPIRE].

[38] X.-G. He, G.C. Joshi, H. Lew and R.R. Volkas, *Simplest Z' model*, *Phys. Rev.* **D 44** (1991) 2118 [INSPIRE].

[39] E. Ma, D.P. Roy and S. Roy, *Gauged L_μ-L_τ with large muon anomalous magnetic moment and the bimaximal mixing of neutrinos*, *Phys. Lett.* **B 525** (2002) 101 [hep-ph/0110146] [INSPIRE].

[40] Z.-Z. Xing and Z.-H. Zhao, *A review of μ-τ flavor symmetry in neutrino physics*, *Rept. Prog. Phys.* **79** (2016) 076201 [arXiv:1512.04207] [INSPIRE].

[41] A. Brignole and A. Rossi, *Anatomy and phenomenology of μ-τ lepton flavor violation in the MSSM*, *Nucl. Phys.* **B 701** (2004) 3 [hep-ph/0404211] [INSPIRE].

[42] R.N. Mohapatra and W. Rodejohann, *Broken μ-τ symmetry and leptonic CP-violation*, *Phys. Rev.* **D 72** (2005) 053001 [hep-ph/0507312] [INSPIRE].

[43] Z.-Z. Xing, H. Zhang and S. Zhou, *Nearly tri-bimaximal neutrino mixing and CP-violation from μ-τ symmetry breaking*, *Phys. Lett.* **B 641** (2006) 189 [hep-ph/0607091] [INSPIRE].

[44] B. Adhikary, *Soft breaking of L_μ-L_τ symmetry: light neutrino spectrum and leptogenesis*, *Phys. Rev.* **D 74** (2006) 033002 [hep-ph/0604009] [INSPIRE].

JHEP09(2016)147

[45] T. Kitabayashi and M. Yasue, *μ-τ symmetry and maximal CP-violation*, *Phys. Lett.* **B 621** (2005) 133 [hep-ph/0504212] [INSPIRE].

[46] S. Baek and P. Ko, *Phenomenology of $\mathrm{U}(1)_{L_\mu - L_\tau}$ charged dark matter at PAMELA and colliders*, *JCAP* **10** (2009) 011 [arXiv:0811.1646] [INSPIRE].

[47] H.-J. He and F.-R. Yin, *Common origin of μ-τ and CP breaking in neutrino seesaw, baryon asymmetry and hidden flavor symmetry*, *Phys. Rev.* **D 84** (2011) 033009 [arXiv:1104.2654] [INSPIRE].

[48] S.-F. Ge, H.-J. He and F.-R. Yin, *Common origin of soft μ-τ and CP breaking in neutrino seesaw and the origin of matter*, *JCAP* **05** (2010) 017 [arXiv:1001.0940] [INSPIRE].

[49] A. Esteban-Pretel, S. Pastor, R. Tomas, G.G. Raffelt and G. Sigl, *μ-τ neutrino refraction and collective three-flavor transformations in supernovae*, *Phys. Rev.* **D 77** (2008) 065024 [arXiv:0712.1137] [INSPIRE].

[50] J. Heeck and W. Rodejohann, *Gauged L_μ-L_τ symmetry at the electroweak scale*, *Phys. Rev.* **D 84** (2011) 075007 [arXiv:1107.5238] [INSPIRE].

[51] A.S. Joshipura, B.P. Kodrani and K.M. Patel, *Fermion masses and mixings in a μ-τ symmetric* SO(10), *Phys. Rev.* **D 79** (2009) 115017 [arXiv:0903.2161] [INSPIRE].

[52] K. Fuki and M. Yasue, *What does μ-tau symmetry imply in neutrino mixings?*, *Phys. Rev.* **D 73** (2006) 055014 [hep-ph/0601118] [INSPIRE].

[53] I. Aizawa and M. Yasue, *A new type of complex neutrino mass texture and μ-τ symmetry*, *Phys. Rev.* **D 73** (2006) 015002 [hep-ph/0510132] [INSPIRE].

[54] B. Adhikary, A. Ghosal and P. Roy, *μ-τ symmetry, tribimaximal mixing and four zero neutrino Yukawa textures*, *JHEP* **10** (2009) 040 [arXiv:0908.2686] [INSPIRE].

[55] W. Grimus and L. Lavoura, *μ-τ interchange symmetry and lepton mixing*, *Fortsch. Phys.* **61** (2013) 535 [arXiv:1207.1678] [INSPIRE].

[56] W. Grimus, S. Kaneko, L. Lavoura, H. Sawanaka and M. Tanimoto, *μ-τ antisymmetry and neutrino mass matrices*, *JHEP* **01** (2006) 110 [hep-ph/0510326] [INSPIRE].

[57] W. Rodejohann and M.A. Schmidt, *Flavor symmetry L_μ-L_τ and quasi-degenerate neutrinos*, *Phys. Atom. Nucl.* **69** (2006) 1833 [hep-ph/0507300] [INSPIRE].

[58] N. Haba and W. Rodejohann, *A supersymmetric contribution to the neutrino mass matrix and breaking of μ-τ symmetry*, *Phys. Rev.* **D 74** (2006) 017701 [hep-ph/0603206] [INSPIRE].

[59] A.S. Joshipura and W. Rodejohann, *Scaling in the neutrino mass matrix, μ-τ symmetry and the see-saw mechanism*, *Phys. Lett.* **B 678** (2009) 276 [arXiv:0905.2126] [INSPIRE].

[60] Z.-Z. Xing and Y.-L. Zhou, *A generic diagonalization of the 3×3 neutrino mass matrix and its implications on the μ-τ flavor symmetry and maximal CP-violation*, *Phys. Lett.* **B 693** (2010) 584 [arXiv:1008.4906] [INSPIRE].

[61] P. Bandyopadhyay, S. Choubey and M. Mitra, *Two Higgs doublet type III seesaw with μ-τ symmetry at LHC*, *JHEP* **10** (2009) 012 [arXiv:0906.5330] [INSPIRE].

[62] W. Grimus, *Realizations of μ-τ interchange symmetry*, *Conf. Proc.* **C 060726** (2006) 312 [hep-ph/0610158] [INSPIRE].

[63] T. Fukuyama and H. Nishiura, *Mass matrix of Majorana neutrinos*, hep-ph/9702253 [INSPIRE].

JHEP09(2016)147

[64] T. Araki and C.Q. Geng, *μ-τ symmetry in Zee-Babu model*, *Phys. Lett.* **B 694** (2011) 113 [arXiv:1006.0629] [INSPIRE].

[65] W.-Z. Feng, P. Nath and G. Peim, *Cosmic coincidence and asymmetric dark matter in a Stückelberg extension*, *Phys. Rev.* **D 85** (2012) 115016 [arXiv:1204.5752] [INSPIRE].

[66] J. Kile, A. Kobach and A. Soni, *Lepton-flavored dark matter*, *Phys. Lett.* **B 744** (2015) 330 [arXiv:1411.1407] [INSPIRE].

[67] J.-C. Park, S.C. Park and J. Kim, *Galactic center GeV gamma-ray excess from dark matter with gauged lepton numbers*, *Phys. Lett.* **B 752** (2016) 59 [arXiv:1505.04620] [INSPIRE].

[68] Z.-H. Zhao, *On the breaking of μ-τ flavor symmetry*, arXiv:1605.04498 [INSPIRE].

[69] S. Patra, S. Rao, N. Sahoo and N. Sahu, *Gauged $\mathrm{U}(1)_{L_\mu - L_\tau}$ model in light of muon $g-2$ anomaly, neutrino mass and dark matter phenomenology*, arXiv:1607.04046 [INSPIRE].

[70] M. Carena, A. Daleo, B.A. Dobrescu and T.M.P. Tait, *Z' gauge bosons at the Tevatron*, *Phys. Rev.* **D 70** (2004) 093009 [hep-ph/0408098] [INSPIRE].

[71] G. Cacciapaglia, C. Csáki, G. Marandella and A. Strumia, *The minimal set of electroweak precision parameters*, *Phys. Rev.* **D 74** (2006) 033011 [hep-ph/0604111] [INSPIRE].

[72] ATLAS collaboration, *Search for high-mass dilepton resonances in pp collisions at $\sqrt{s} = 8$ TeV with the ATLAS detector*, *Phys. Rev.* **D 90** (2014) 052005 [arXiv:1405.4123] [INSPIRE].

[73] W. Altmannshofer, S. Gori, M. Pospelov and I. Yavin, *Neutrino trident production: a powerful probe of new physics with neutrino beams*, *Phys. Rev. Lett.* **113** (2014) 091801 [arXiv:1406.2332] [INSPIRE].

[74] Particle Data Group collaboration, K.A. Olive et al., *Review of particle physics*, *Chin. Phys.* **C 38** (2014) 090001 [INSPIRE].

[75] F. Jegerlehner and A. Nyffeler, *The muon $g-2$*, *Phys. Rept.* **477** (2009) 1 [arXiv:0902.3360] [INSPIRE].

[76] S.N. Gninenko and N.V. Krasnikov, *The muon anomalous magnetic moment and a new light gauge boson*, *Phys. Lett.* **B 513** (2001) 119 [hep-ph/0102222] [INSPIRE].

[77] S. Baek, N.G. Deshpande, X.G. He and P. Ko, *Muon anomalous $g-2$ and gauged L_μ-L_τ models*, *Phys. Rev.* **D 64** (2001) 055006 [hep-ph/0104141] [INSPIRE].

[78] Muon g-2 collaboration, G.W. Bennett et al., *Measurement of the negative muon anomalous magnetic moment to 0.7 ppm*, *Phys. Rev. Lett.* **92** (2004) 161802 [hep-ex/0401008] [INSPIRE].

[79] S. Mohanty, S. Rao and D.P. Roy, *Reconciling the muon $g-2$ and dark matter relic density with the LHC results in nonuniversal gaugino mass models*, *JHEP* **09** (2013) 027 [arXiv:1303.5830] [INSPIRE].

[80] S.P. Das, M. Guchait and D.P. Roy, *Testing SUSY models for the muon $g-2$ anomaly via chargino-neutralino pair production at the LHC*, *Phys. Rev.* **D 90** (2014) 055011 [arXiv:1406.6925] [INSPIRE].

[81] W. Altmannshofer, C.-Y. Chen, P.S.B. Dev and A. Soni, *Lepton flavor violating Z' explanation of the muon anomalous magnetic moment*, arXiv:1607.06832 [INSPIRE].

[82] E. Ma, *Verifiable radiative seesaw mechanism of neutrino mass and dark matter*, *Phys. Rev.* **D 73** (2006) 077301 [hep-ph/0601225] [INSPIRE].

JHEP09(2016)147

[83] S. Baek, H. Okada and K. Yagyu, *Flavour dependent gauged radiative neutrino mass model*, *JHEP* **04** (2015) 049 [arXiv:1501.01530] [INSPIRE].

[84] S. Baek, *Dark matter and muon* $(g-2)$ *in local* $\mathrm{U}(1)_{L_\mu - L_\tau}$*-extended Ma model*, *Phys. Lett.* **B 756** (2016) 1 [arXiv:1510.02168] [INSPIRE].

[85] P. Minkowski, $\mu \to e\gamma$ *at a rate of one out of* 10^9 *muon decays?*, *Phys. Lett.* **B 67** (1977) 421 [INSPIRE].

[86] T. Yanagida, *Horizontal symmetry and masses of neutrinos*, *Conf. Proc.* **C 7902131** (1979) 95 [INSPIRE].

[87] R.N. Mohapatra and G. Senjanović, *Neutrino mass and spontaneous parity violation*, *Phys. Rev. Lett.* **44** (1980) 912 [INSPIRE].

[88] J. Schechter and J.W.F. Valle, *Neutrino masses in* $\mathrm{SU}(2) \times \mathrm{U}(1)$ *theories*, *Phys. Rev.* **D 22** (1980) 2227 [INSPIRE].

[89] S. Choubey and W. Rodejohann, *A flavor symmetry for quasi-degenerate neutrinos:* L_μ*-*L_τ, *Eur. Phys. J.* **C 40** (2005) 259 [hep-ph/0411190] [INSPIRE].

[90] ATLAS collaboration, *Observation of a new particle in the search for the Standard Model Higgs boson with the ATLAS detector at the LHC*, *Phys. Lett.* **B 716** (2012) 1 [arXiv:1207.7214] [INSPIRE].

[91] CMS collaboration, *Observation of a new boson at a mass of* 125 *GeV with the CMS experiment at the LHC*, *Phys. Lett.* **B 716** (2012) 30 [arXiv:1207.7235] [INSPIRE].

[92] A. Biswas, S. Choubey and S. Khan, *Galactic gamma ray excess and dark matter phenomenology in a* $\mathrm{U}(1)_{B-L}$ *model*, *JHEP* **08** (2016) 114 [arXiv:1604.06566] [INSPIRE].

[93] N. Chakrabarty, D.K. Ghosh, B. Mukhopadhyaya and I. Saha, *Dark matter, neutrino masses and high scale validity of an inert Higgs doublet model*, *Phys. Rev.* **D 92** (2015) 015002 [arXiv:1501.03700] [INSPIRE].

[94] CHARM-II collaboration, D. Geiregat et al., *First observation of neutrino trident production*, *Phys. Lett.* **B 245** (1990) 271 [INSPIRE].

[95] CCFR collaboration, S.R. Mishra et al., *Neutrino tridents and* WZ *interference*, *Phys. Rev. Lett.* **66** (1991) 3117 [INSPIRE].

[96] B. Adhikary, M. Chakraborty and A. Ghosal, *Masses, mixing angles and phases of general Majorana neutrino mass matrix*, *JHEP* **10** (2013) 043 [*Erratum ibid.* **09** (2014) 180] [arXiv:1307.0988] [INSPIRE].

[97] J. Edsjo and P. Gondolo, *Neutralino relic density including coannihilations*, *Phys. Rev.* **D 56** (1997) 1879 [hep-ph/9704361] [INSPIRE].

[98] A. Biswas and D. Majumdar, *The real gauge singlet scalar extension of Standard Model: a possible candidate of cold dark matter*, *Pramana* **80** (2013) 539 [arXiv:1102.3024] [INSPIRE].

[99] J.M. Cline, K. Kainulainen, P. Scott and C. Weniger, *Update on scalar singlet dark matter*, *Phys. Rev.* **D 88** (2013) 055025 [*Erratum ibid.* **D 92** (2015) 039906] [arXiv:1306.4710] [INSPIRE].

[100] G. Bélanger, F. Boudjema, A. Pukhov and A. Semenov, *MicrOMEGAs*$_3$*: a program for calculating dark matter observables*, *Comput. Phys. Commun.* **185** (2014) 960 [arXiv:1305.0237] [INSPIRE].

JHEP09(2016)147

[101] A. Semenov, *LanHEP: a package for the automatic generation of Feynman rules in field theory. Version* 3.0, *Comput. Phys. Commun.* **180** (2009) 431 [arXiv:0805.0555] [INSPIRE].

[102] P. Bechtle, S. Heinemeyer, O. Stål, T. Stefaniak and G. Weiglein, *Probing the Standard Model with Higgs signal rates from the Tevatron, the LHC and a future ILC*, *JHEP* **11** (2014) 039 [arXiv:1403.1582] [INSPIRE].

[103] DARWIN collaboration, J. Aalbers et al., *DARWIN: towards the ultimate dark matter detector*, arXiv:1606.07001 [INSPIRE].

[104] L. Goodenough and D. Hooper, *Possible evidence for dark matter annihilation in the inner milky way from the Fermi gamma ray space telescope*, arXiv:0910.2998 [INSPIRE].

[105] D. Hooper and L. Goodenough, *Dark matter annihilation in the galactic center as seen by the Fermi gamma ray space telescope*, *Phys. Lett.* **B 697** (2011) 412 [arXiv:1010.2752] [INSPIRE].

[106] A. Boyarsky, D. Malyshev and O. Ruchayskiy, *A comment on the emission from the galactic center as seen by the Fermi telescope*, *Phys. Lett.* **B 705** (2011) 165 [arXiv:1012.5839] [INSPIRE].

[107] D. Hooper and T. Linden, *On the origin of the gamma rays from the galactic center*, *Phys. Rev.* **D 84** (2011) 123005 [arXiv:1110.0006] [INSPIRE].

[108] K.N. Abazajian and M. Kaplinghat, *Detection of a gamma-ray source in the galactic center consistent with extended emission from dark matter annihilation and concentrated astrophysical emission*, *Phys. Rev.* **D 86** (2012) 083511 [*Erratum ibid.* **D 87** (2013) 129902] [arXiv:1207.6047] [INSPIRE].

[109] D. Hooper and T.R. Slatyer, *Two emission mechanisms in the Fermi bubbles: a possible signal of annihilating dark matter*, *Phys. Dark Univ.* **2** (2013) 118 [arXiv:1302.6589] [INSPIRE].

[110] K.N. Abazajian, N. Canac, S. Horiuchi and M. Kaplinghat, *Astrophysical and dark matter interpretations of extended gamma-ray emission from the galactic center*, *Phys. Rev.* **D 90** (2014) 023526 [arXiv:1402.4090] [INSPIRE].

[111] T. Daylan et al., *The characterization of the gamma-ray signal from the central milky way: a case for annihilating dark matter*, *Phys. Dark Univ.* **12** (2016) 1 [arXiv:1402.6703] [INSPIRE].

[112] B. Zhou et al., *GeV excess in the milky way: the role of diffuse galactic gamma-ray emission templates*, *Phys. Rev.* **D 91** (2015) 123010 [arXiv:1406.6948] [INSPIRE].

[113] FERMI-LAT collaboration, M. Ajello et al., *Fermi-LAT observations of high-energy γ-ray emission toward the galactic center*, *Astrophys. J.* **819** (2016) 44 [arXiv:1511.02938] [INSPIRE].

[114] P. Agrawal, B. Batell, P.J. Fox and R. Harnik, *WIMPs at the galactic center*, *JCAP* **05** (2015) 011 [arXiv:1411.2592] [INSPIRE].

[115] A. Berlin, D. Hooper and S.D. McDermott, *Simplified dark matter models for the galactic center gamma-ray excess*, *Phys. Rev.* **D 89** (2014) 115022 [arXiv:1404.0022] [INSPIRE].

[116] A. Biswas, D. Majumdar and P. Roy, *Nonthermal two component dark matter model for Fermi-LAT γ-ray excess and* 3.55 *keV X-ray line*, *JHEP* **04** (2015) 065 [arXiv:1501.02666] [INSPIRE].

JHEP09(2016)147

[117] J.F. Navarro, C.S. Frenk and S.D.M. White, *A universal density profile from hierarchical clustering*, *Astrophys. J.* **490** (1997) 493 [astro-ph/9611107] [INSPIRE].

[118] M. Cirelli et al., *PPPC 4 DM ID: a Poor Particle Physicist Cookbook for Dark Matter Indirect Detection*, *JCAP* **03** (2011) 051 [*Erratum ibid.* **10** (2012) E01] [arXiv:1012.4515] [INSPIRE].

[119] F. Calore, I. Cholis and C. Weniger, *Background model systematics for the Fermi GeV excess*, *JCAP* **03** (2015) 038 [arXiv:1409.0042] [INSPIRE].

JHEP09(2016)147